

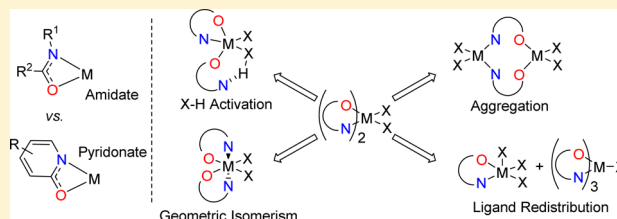
Bis(*tert*-butylimido)bis(*N,O*-chelate)tungsten(VI) Complexes: Probing Amidate and Pyridonate Hemilability

Joseph M. Clarkson and Laurel L. Schafer*[✉]

Department of Chemistry, University of British Columbia, 2036 Main Mall, Vancouver, British Columbia V6T 1Z1, Canada

S Supporting Information

ABSTRACT: Four new bis(*tert*-butylimido)bis(*N,O*-chelate)tungsten(VI) complexes (3–6), in which the *N,O*-chelate is an amidate or pyridonate ligand, have been synthesized and characterized. Computational analysis has been used to calculate the relative energies of different stereoisomers and shown how the steric demand of each ligand influences coordination and bonding modes. The electronically saturated complexes have been employed to evaluate 1,3-*N,O*-chelated metal–ligand interactions. Complexes 3–6 were treated with electrophilic reagents, which resulted in strikingly different reactivity patterns between the amidate and the pyridonate ligated complexes. The observed reactivity differences are accompanied by direct observation of different trends in the hemilability of these two different classes of 1,3-*N,O*-chelates.



INTRODUCTION

The term hemilabile ligands was coined in 1979 when Jeffrey and Rauchfuss reported the metal–ligand interactions of (2-methoxyphenyl)diphenylphosphine coordinated to ruthenium.¹ A hemilabile ligand is a chelated ligand that readily dissociates an atom of the chelate from the metal center, leaving another part of the chelate still bound to the metal center. This ligand can then reveal a coordination site at the metal center, allowing a substrate to bind for subsequent reactivity, sensing, or stabilization.² We have shown that 1,3-*N,O*-chelating ligands, such as amidate, pyridonate, ureate, phosphoramidate, and sulfonamide ligands, can adopt different bonding modes and participate in E–H (where E = B, C, N, and O) bond activations.^{3–5} 1,3-*N,O*-Chelate hemilability is described as a change in bonding mode between κ^2 -*N,O* and/or μ^2 -*N,O* to either κ^1 -*N* or κ^1 -*O* (Figure 1).

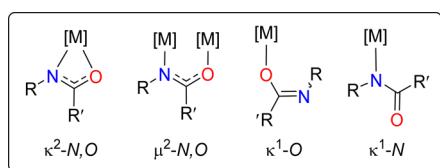


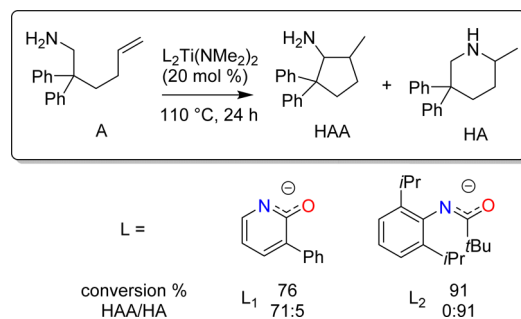
Figure 1. Observed binding modes of 1,3-*N,O*-chelated ligands, which highlight ligand hemilability.

These 1,3-*N,O*-chelating ligands (i.e., amidate and pyridonate) are unique from the traditional hemilabile ligands first described by Jeffrey and Rauchfuss in that they do not have a strictly inert donor (*P*) and a labile donor (*O*); rather, both the *N* and the *O* of the 1,3-*N,O*-chelate can act as either inert or labile donors (i.e., κ^1 -*N* or κ^1 -*O* can be accessed).¹ Solid-state molecular structures in which the 1,3-*N,O*-chelate adopts κ^2 -*N,O*, κ^1 -*O*, κ^1 -*N*, and μ^2 -*N,O* bonding modes have been

observed across the periodic table;⁶ however, the rapid changes in bonding modes make it difficult to observe different coordination environments in solution by NMR spectroscopy. To date, only a few experimental studies have reported the observation of discrete amidate or pyridonate hemilabile coordination environments in solution.^{7–11}

These 1,3-*N,O*-chelating ligands can support high-valent early transition metals which are competent catalysts for hydroamination (HA)^{12–20} and hydroaminoalkylation (HAA)^{21–26} reactions. These hydrofunctionalization reactions, hydroamination (a C–N bond forming reaction),^{27,28} and hydroaminoalkylation (a C–C bond forming reaction),²⁹ are catalytic transformations targeting improved atom economy and efficiency in the synthesis of amine-containing fine chemicals.³⁰ For example, an amidate-supported titanium catalyst is capable of realizing anti-Markovnikov hydroamination of terminal alkenes with primary amines with a broad range of substrates.^{16,31–33} The observed exquisite regioselectivity is proposed to be due to the hemilability of the amidate ligand.³⁴ In another example we have taken advantage of the difference between the hemilability of amidates vs pyridonates to develop catalyst-controlled chemoselectivity of intramolecular hydroaminoalkylation with primary aminoalkene substrates (e.g., L₁, Scheme 1) over intramolecular hydroamination (e.g., L₂, Scheme 1).³⁵ Thus, the variable hemilability of these two classes of 1,3-*N,O*-chelating ligands supports divergent catalytic pathways by allowing access to multiple bonding and coordination modes. Consequently, we proposed that pyridonate ligands are more hemilabile than amidate ligands and thus are more prone to forming dynamic systems with a diverse array of bonding modes under catalytic

Received: December 7, 2016

Scheme 1. Hydrofunctionalization of A^a

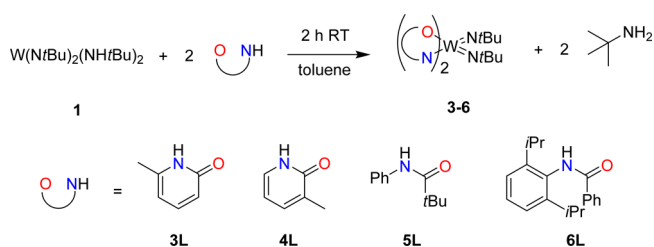
^aDepending upon the 1,3-*N,O*-chelate employed the hydroaminoalkylation (HAA) or hydroamination (HA) product can be preferentially accessed. This change in product distribution has been proposed to be rationalized by ligand hemilability.^{35,36}

reaction conditions.^{11,35–37} These differences between pyridonate and amidate ligands have been proposed to stem from steric features, which in turn impact the hemilability of the ligand.^{34,38} Thus, by understanding the trends in ligand hemilability, this feature can be incorporated as a ligand design element for promoting improved or new reactivity.

In the aforementioned systems the 1,3-*N,O*-chelating ligands are auxiliary ligands used to modify the reactivity at the metal center. In this work, we sought a system where the *N,O*-chelates would be more reactive than the other ligands on the metal in order to observe structure and reactivity effects of different 1,3-*N,O*-chelating ligands. This approach would allow us to observe effects of temperature, coordination of additional donors, and proton shuttling on 1,3-*N,O*-chelated complexes. To this end, the bis(*tert*-butylimido)X₂tungsten(VI) framework (where X is a monoanionic ligand) is an ideal system for such investigations because (1) the covalent radii of titanium and tungsten are nearly identical,^{39,40} (2) the bis(*tert*-butylimido)tungsten system has nitrogen-donating atoms that have significant M–N π bonding, similar to the bis(dimethylamido)bis(*N,O*-chelate)titanium(IV) complexes used in the aforementioned catalytic reactions, (3) the bis(*tert*-butylimido)bis(*N,O*-chelate)tungsten framework, with its pseudo-octahedral geometry, will mimic the geometric environment of the bis(dimethylamido)-bis(*N,O*-chelate)titanium(IV) complexes, and (4) simple protonolysis routes from suitable tungsten(VI) precursors have been devised.⁴¹ Although the absolute metal–ligand interactions of new *N,O*-chelated tungsten complexes will be different from the known *N,O*-chelated titanium systems (i.e., quantitative equilibrium constants of a hemilabile *N,O*-chelate exchanging from κ^2 -*N,O* to κ^1 -*O*), the similarities between the two systems would allow for observation of relative trends in *N,O*-chelates on high-valent early transition metal complexes.

To date, there have been only a handful of monomeric 1,3-*N,O*-chelated tungsten complexes reported.^{41–46} Two bis(imido)bis(*N,O*-chelate)tungsten complexes have been reported previously; however, neither was structurally characterized nor were their reactivities reported.^{41,46} Here a series of bis(*tert*-butylimido)bis(*N,O*-chelate)tungsten(VI) complexes (Scheme 2) allows for systematic investigations of steric and electronic effects on the hemilability of various 1,3-*N,O*-chelated ligands.

We report herein the synthesis, characterization, and reactivity investigations of a series of new bis(*tert*-butylimido)-bis(*N,O*-chelate)tungsten(VI) complexes. Computational in-

Scheme 2. Synthesis of 1,3-*N,O*-Chelated Tungsten Complexes via Protonolysis Reactions (top) and Corresponding Proligands (bottom)

vestigations and reactivity studies of bis(*tert*-butylimido)bis(*N,O*-chelate)tungsten complexes illustrate the enhanced hemilability of pyridonate ligands in comparison to amidates. Furthermore, the steric demand of each unique ligand also imparts a variable degree of hemilabile character and influences coordination and bonding modes. These insights correlate to reported reactivity trends in established 1,3-*N,O*-chelated hydroamination and hydroaminoalkylation catalytic systems. Finally, predictive guidance for selecting preferred ligands in the development of improved catalysts or new reactivity is provided.

EXPERIMENTAL SECTION

All reactions were conducted under an inert atmosphere of nitrogen, inside a glovebox, or using standard Schlenk techniques unless otherwise noted. All chemicals were purchased from commercial sources and used as received unless otherwise noted. Bis(*tert*-butylimido)bis(*tert*-butylimido)tungsten(VI) was prepared according to the published procedure.⁴⁷ Trimethylsilyl chloride was distilled under nitrogen and stored in a Teflon-sealed Schlenk tube. Amide proligands 5L and 6L were synthesized from commercially available acid chlorides and primary amines by published procedures.¹⁶ Proligands were sublimed or dried under high vacuum overnight. All solvents (excluding deuterated solvents) were passed through an activated alumina tower. Benzene-*d*₆ and toluene-*d*₈ were dried over sodium metal and distilled. NMR spectra were obtained on a Bruker Avance 300 spectrometer, a Bruker Avance 400mv spectrometer, or a Bruker Avance 400dir spectrometer. EI mass spectra were acquired on a Kratos MS-50 spectrometer. Elemental analyses were collected on a Carlo Erba Elemental Analyzer EA 1108 instrument. GC/MS were conducted on an Agilent 7890A GC equipped with a 5975C inert XL EI/CI mass detector which is operated in positive CI mode with methane as the reagent gas.

Lutidinium Hydrochloride. 2,6-Dimethylpyridine (1.422 g, 0.01327 mol) was dissolved in 5 mL of hexanes in a 25 mL RBF, open to air. A dropwise addition of 5 mL of a 4 M HCl in a diethyl ether solution was added to the solution of 2,6-dimethylpyridine at 0 °C while stirring. A white solid immediately formed upon addition of the HCl solution. The white solid was isolated by filtration and washed twice with 10 mL of Et₂O. The lutidinium hydrochloride was dried under vacuum overnight and then sublimed. The resulting solid was a colorless solid. Yield: 1.773 g, 93%. ¹H NMR (DMSO-*d*₆, 300 MHz): δ = 8.33 (t, *J* = 7.9 Hz, 1 H), 7.70 (d, *J* = 7.9 Hz, 2 H), 2.75 ppm (s, 6 H).

Bis(*tert*-butylimido)bis(κ^2 -*N,O*)-6-methyl-2-pyridonate)tungsten(VI) (3). Complex 1 (0.4710 g, 1.001 mmol) was dissolved in 6 mL of toluene and then added to a vial charged with 6-methyl-2-pyridone (0.2190 g, 2.007 mmol) and a stir bar. The mixture was capped and stirred for 2 h, resulting in a translucent yellow solution. The volatiles were then removed under vacuum, and the resulting yellow semisolid was dissolved in 7.5 mL of hexanes and filtered through a 1 cm bed of Celite. The volatiles were again removed under vacuum to yield a yellow semisolid. The semisolid was dissolved in hexanes, shaken, and then dried under vacuum, again yielding a yellow semisolid. The

yellow semisolid turned to a crystalline solid after days in a capped vial at room temperature. Yield: 0.5170 g, 95%. ^1H NMR (400 MHz, benzene- d_6) δ = 6.91 (dd, J = 7.3, 8.3 Hz, 2 H), 6.26 (d, J = 8.3 Hz, 2 H), 6.01 (d, J = 7.3 Hz, 2 H), 2.11 (s, 6 H), 1.48 (s, 18 H); ^{13}C NMR (75 MHz, benzene- d_6) δ = 172.1, 153.3, 140.7, 113.2, 107.3, 67.0, 33.2, 21.8; MS(EI) m/z 542 ($[\text{M}]^+$), m/z 527 ($[\text{M} - \text{Me}]^+$), m/z 471 ($[\text{M} - \text{NtBu}]^+$), m/z 414 ($[\text{M} - \text{NtBu} - \text{tBu}]^+$). Anal. Calcd for $\text{WO}_2\text{N}_4\text{C}_{20}\text{H}_{30}$: N, 10.33; C, 44.29; H, 5.58. Found: N, 9.97; C, 44.53; H, 5.66.

Bis(tert-butylimido)bis((κ^2 -N,O)3-methyl-2-pyridonate)tungsten(VI) (4). Complex 1 (0.2357 g, 0.5011 mmol) was dissolved in 3 mL of toluene and then added to a vial charged with 3-methyl-2-pyridone (0.1110 g, 1.017 mmol) and a stir bar. The mixture was capped and stirred for 2 h, resulting in a translucent yellow solution. The volatiles were then removed under vacuum, and the resulting yellow semisolid was dissolved in 4 mL of hexanes and filtered through a bed of Celite. The volatiles were again removed under vacuum to yield a yellow semisolid, which was recrystallized from minimal warm hexanes at -35 °C overnight and afforded a bright yellow powder. The mother liquor was decanted, and the solids were dried under vacuum. Yield: 0.2065 g, 76%. ^1H NMR (300 MHz, benzene- d_6) δ = 7.62 (d, J = 5.6 Hz, 2 H), 6.82 (d, J = 7.0 Hz, 2 H), 6.06 (dd, J = 5.6, 7.0 Hz, 2 H), 1.94 (s, 6 H), 1.44 (s, 18 H); ^{13}C NMR (75 MHz, benzene- d_6) δ = 172.9, 141.6, 140.0, 123.0, 112.0, 67.2, 33.2, 15.1; MS(EI) m/z 542 ($[\text{M}]^+$), m/z 527 ($[\text{M} - \text{Me}]^+$), m/z 471 ($[\text{M} - \text{NtBu}]^+$), m/z 414 ($[\text{M} - \text{NtBu} - \text{tBu}]^+$). Anal. Calcd for $\text{WO}_2\text{N}_4\text{C}_{26}\text{H}_{30}$: N, 10.33; C, 44.29; H, 5.58. Found: N, 10.31; C, 44.60; H, 5.43.

Bis(tert-butylimido)bis((κ^2 -N,O)N-phenylpivalamide)tungsten(VI) (5). Complex 1 (0.2014 g, 0.4282 mmol) was dissolved in 4 mL of toluene and then added to a vial charged with N-phenylpivalamide (0.1473 g, 0.8310 mmol) and a stir bar. The resulting mixture was capped and stirred for 2 h, resulting in a translucent yellow solution. The volatiles were then removed under vacuum to give a pale yellow crystalline solid. The solids were recrystallized from minimal warm hexanes at ambient temperature overnight. Large yellow prisms formed, the mother liquor was decanted, and a second batch of crystals formed after the mother liquor was stored in a -35 °C freezer overnight to yield smaller yellow prisms. The yellow crystals were dried under vacuum. Yield: 0.2257 g, 80%. ^1H NMR (400 MHz, benzene- d_6): δ = 7.26 (d, J = 6.1 Hz, 4 H), 7.05 (apparent t, J = 7.5 Hz, 4 H), 6.88 (t, J = 7.5 Hz, 2 H), 1.16 (br. s, 18 H), 1.15 ppm (br. s, 18 H); ^{13}C NMR (101 MHz, benzene- d_6) δ = 188.6, 149.4, 128.8, 127.9, 125.8, 66.5, 42.5, 32.7, 28.6; MS(EI) m/z 678 ($[\text{M} - \text{Me}]^+$), m/z 663 ($[\text{M} - \text{Me}]^+$). Anal. Calcd for $\text{WO}_2\text{N}_4\text{C}_{30}\text{H}_{36}$: N, 8.25; C, 53.10; H, 6.83. Found: N, 7.97; C, 53.27; H, 6.69.

Bis(tert-butylimido)bis((κ^2 -N,O)N-(2,6-diisopropylphenyl)benzamide)tungsten(VI) (6). Complex 1 (0.2348 g, 0.4992 mmol) was dissolved in 4.5 mL of toluene and then added to a vial charged with N-(2,6-diisopropylphenyl)benzamide (0.2846 g, 1.011 mmol) and a stir bar. The mixture was capped and stirred for 2 h, resulting in a translucent yellow solution. The volatiles were then removed under vacuum, producing a yellow crystalline solid. The crystalline solids were dissolved in 10 mL hexanes and filtered through a plug of Celite. The volatiles were removed, leaving analytically pure yellow crystalline solids. Yield: 0.3799 g, 86%. ^1H NMR (300 MHz, benzene- d_6) δ = 7.76 (dd, J = 1.5, 8.3 Hz, 4 H), 7.29–7.18 (m, 6 H), 6.94–6.79 (m, 6 H), 4.19 (spt, J = 6.9 Hz, 2 H), 3.90 (spt, J = 6.9 Hz, 2 H), 1.74 (d, J = 6.9 Hz, 6 H), 1.44 (d, J = 6.9 Hz, 6 H), 1.20 (s, 18 H), 1.15 (d, J = 6.9 Hz, 6 H), 0.96 (d, J = 6.9 Hz, 6 H); ^{13}C NMR (75 MHz, benzene- d_6) δ = 178.5, 145.0, 144.0, 143.7, 134.1, 132.1, 130.4, 127.7, 125.4, 124.0, 67.6, 32.7, 28.5, 28.4, 26.5, 25.4, 24.0, 23.3; MS(EI) m/z 886 ($[\text{M}]^+$), m/z 871 ($[\text{M} - \text{Me}]^+$). Anal. Calcd for $\text{WO}_2\text{N}_4\text{C}_{20}\text{H}_{30}$: N, 6.32; C, 62.30; H, 7.05. Found: N, 6.72; C, 62.67; H, 7.14.

(tert-Butylimido)(tert-butylimido)bis((κ^1 -O)6-methyl-2-pyridonate)((κ^2 -N,O)6-methyl-2-pyridonate)tungsten(VI) (7). Solid complex 7 was precipitated from an equilibrium mixture of pyridonate complex 3 (0.0500 g, 0.09713 mmol) and proligand 3L (0.0106 g, 0.09220 mmol) in hexanes at -35 °C. The mother liquor was decanted, and the solids were dried under reduced pressure. ^1H NMR (300 MHz, benzene- d_6): δ = 6.93 (dd, J = 7.4, 8.2 Hz, 2 H), 6.79 (dd, J

= 6.9, 9.1 Hz, 1 H), 6.38 (d, J = 9.1 Hz, 1 H), 6.28 (d, J = 8.2 Hz, 2 H), 6.03 (d, J = 7.4 Hz, 2 H), 5.47 (d, J = 6.9 Hz, 1 H), 2.14 (s, 6 H), 2.00 (s, 3 H), 1.47 (s, 18 H); ^{13}C NMR (75 MHz, benzene- d_6): δ = 172.0, 167.2, 153.5, 147.5, 141.5, 140.6, 116.6, 113.3, 107.5, 106.3, 66.7, 33.1, 22.0, 19.5; MS(EI) m/z 579 $[\text{M} - \text{HNtBu}]^+$, m/z 523 $[\text{M} - \text{HNtBu} - \text{C}_3\text{H}_8]^+$. Anal. Calcd for $\text{WO}_3\text{N}_5\text{C}_{26}\text{H}_{37}$: N, 10.75; C, 47.94; H, 5.72. Found: N, 10.64; C, 48.03; H, 5.69.

(tert-Butylimido)(tert-butylimido)tris(3-methyl-2-pyridonate)tungsten(VI) (8). Precipitation of white and yellow solids from an equilibrium mixture of pyridonate complex 4 and proligand 4L does not produce a single isolable product. EIMS conducted on the precipitated solids showed fragments corresponding to complex 4 and a (tert-butylimido)tris(3-methyl-2-pyridonate)tungsten(VI) fragment. The ^1H NMR solution-phase spectrum suggested fluxional species, which was confirmed by variable-temperature ^1H NMR spectroscopy experiments. ^1H NMR 25 °C (400 MHz, toluene- d_8) δ = 8.43 (br s), 8.06 (br s), 7.79 (d, J = 4.9 Hz), 7.76 (d, J = 4.9 Hz), 7.40 (d, J = 4.4 Hz), 6.87 (d, J = 7.3 Hz), 6.33–6.25 (m), 6.15 (dd, J = 5.4, 6.8 Hz), 6.02 (t, J = 6.1 Hz), 2.56 (br s), 1.99 (br s), 1.97 (s), 1.93 (s), 1.41 (s), 1.02 (s), 0.99 (s); MS(EI) m/z 579 $[\text{M} - \text{HNtBu}]^+$, m/z 523 $[\text{M} - \text{HNtBu} - \text{C}_3\text{H}_8]^+$.

Bis(tert-butylimido)chloro((κ^2 -N,O)N-phenyl)pivalamidate)tungsten(VI) (9) and (tert-butylimido)(tert-butylimido)dichloro(N-phenylpivalamidate)tungsten(VI) (10). Complex 5 (0.0509 g, 0.0750 mmol) was dissolved in 2 mL of toluene and added to a vial containing a suspension of lutidinium hydrochloride (0.0114 g, 0.0794 mmol) in 2 mL of toluene in a glovebox. The yellow mixture was then stirred at ambient temperature for 4 h. The volatiles were removed to yield pale yellow solids. Hexanes (1.5 mL) was used to form a suspension of the crude solids, which was filtered through a 2 cm plug of Celite, and the volatiles were removed under vacuum. The filtration was conducted again using 1.5 mL of hexanes and again filtering through a 2 cm plug of Celite, and the volatiles were removed under vacuum. The solids were dissolved in warm hexanes and recrystallized at room temperature, colorless crystals formed overnight, the mother liquor was decanted, and the crystals were dried under vacuum. This first batch of crystalline material yielded small amounts (less than 0.01 g) of predominately complex 10, contaminated with complex 9 and proligand 5L. The mother liquor was decanted, concentrated, and then left to recrystallize again for 2 days, yielding colorless crystalline rods which were found to be complex 9 (0.0096 g) contaminated with proligand 5L and small amounts of complex 10. The mother liquor was decanted, and the crystals were dried in vacuum. Analytically pure material of complex 9 or 10 could not be obtained. ^1H NMR spectra of the recrystallized complexes 9 and 10 are shown in the Supporting Information (Figures S29 and S30, respectively). Spectroscopic assignments for complex 9: ^1H NMR (300 MHz, benzene- d_6): δ = 7.08–6.95 (m, 4 H), 6.83 (tt, J = 2.1, 7.2 Hz, 1 H), 1.27 (s, 18 H), 0.91 (s, 9 H); MS(EI) m/z 537 $[\text{M}]^+$, m/z 522 $[\text{M} - \text{Me}]^+$. Spectroscopic assignments for complex 10: ^1H NMR (300 MHz, benzene- d_6) δ ppm 1.02 (s, 9 H) 1.09 (s, 9 H) 1.16 (s, 9 H) 6.92 (tt, J = 7.4, 1.3 Hz, 1 H) 7.06–7.13 (m, 2 H) 7.59–7.65 (m, 2 H) 9.87 (br s, 1 H)

(tert-Butylimido)(chloro)bis((κ^1 -O)6-methyl-2-pyridonate)((κ^2 -N,O)6-methyl-2-pyridonate)tungsten(VI) (11). Complex 3 (0.0360 g, 0.06638 mmol) was dissolved in 3 mL of toluene and added to a vial containing solid lutidinium hydrochloride (0.0093 g, 0.06476 mmol) in a glovebox. The mixture was stirred at ambient temperature for 4 h; then 3 mL of hexanes was added and the stirring was halted. Off-white solids precipitated, and the mother liquor was decanted. The solids were washed with 2 mL of hexanes twice, and then the solids were dried under vacuum. Yield: 0.0087 g. Analytically pure material of complex 11 could not be obtained. The ^1H NMR spectrum of the recrystallized complex 11 is shown in the Supporting Information (Figure S31). ^1H NMR (300 MHz, benzene- d_6) δ = 6.99 (t, J = 7.9 Hz, 3 H), 6.59–6.09 (m, 6 H), 2.54 (s, 9 H), 1.09 (s, 9 H); MS(EI) m/z 579 $[\text{M} - \text{Cl}]^+$, m/z 506 $[\text{M} - \text{ONC}_6\text{H}_6]^+$, m/z 472 $[\text{M} - \text{ONC}_6\text{H}_6 - \text{Cl}]^+$, m/z 450 $[\text{M} - \text{ONC}_6\text{H}_6 - \text{C}_3\text{H}_8]^+$, m/z 414 $[\text{M} - \text{ONC}_6\text{H}_6 - \text{Cl} - \text{C}_3\text{H}_8]^+$.

Bis(tert-butylimido)chloro((κ^2 -N,O)6-methyl-2-pyridonate)tungsten(VI) (12). Complex 3 (0.0637 g, 0.118 mmol) was dissolved in 1.5 mL

of toluene and added to a Teflon sealable reaction flask that was charged with a stir bar. The reaction vessel was then taken out of the glovebox, and 1.2 mL of 0.15 M TMSCl (0.020 g, 0.18 mmol) in toluene was added via syringe to the reaction flask on a Schlenk line. The reaction flask was put in a 60 °C oil bath. The mixture was stirred for 20 h, during which the color changed from a yellow solution to an orange color. The reaction was then removed from the oil bath and allowed to cool to room temperature. The volatiles were then removed under vacuum, affording a red solid. The reaction flask was taken back into the glovebox, and the solids were extracted with hexanes (4–5 mL) and filtered through the a Celite plug; then the volatiles were removed. The solids were recrystallized from warm hexanes at room temperature overnight, producing colorless crystalline solids. The mother liquor was decanted, and the solids were washed with cold hexanes and then dried under vacuum. Yield: 0.0157 g. Analytically pure material of complex **12** could not be obtained. The ¹H NMR spectrum of the recrystallized complex **12** is shown in the Supporting Information (Figure S32). ¹H NMR (300 MHz, benzene-*d*₆) δ = 6.74 (dd, *J* = 7.5, 8.7 Hz, 1 H), 5.94 (d, *J* = 8.7 Hz, 1 H), 5.89 (d, *J* = 7.5 Hz, 1 H), 1.96 (br s, 3 H), 1.31 (s, 18 H); MS(EI) *m/z* 469 [M]⁺, *m/z* 454 [M – Me]⁺, *m/z* 398 [M – NtBu]⁺.

Bis(tert-butylimido)chloro((κ²-N,O)3-methyl-2-pyridonate)tungsten (13). Complex **4** (0.0502 g, 0.0926 mmol) was dissolved in 2 mL of toluene and added to a Teflon sealable reaction flask that was charged with a stir bar in the glovebox. The reaction vessel was taken out of the glovebox, and 0.6 mL of TMSCl (0.5 g, 5 mmol) was added via a syringe to the flask on a Schlenk line. The reaction flask was then put in a 60 °C oil bath. The mixture was stirred for 20 h, during which the color of the solution remained yellow. The reaction was then removed from the oil bath and allowed to cool to room temperature. The volatiles were then removed under vacuum, leaving a yellow solid. The reaction flask was taken back into the glovebox, and the solids were dissolved in minimal warm toluene and recrystallized at room temperature overnight, producing small pale yellow crystals. The mother liquor was decanted, and the solids were dried under vacuum. Yield: 0.0242 g. Analytically pure material of complex **13** could not be obtained. The ¹H NMR spectrum of the recrystallized complex **13** is shown in the Supporting Information (Figure S33). ¹H NMR (300 MHz, benzene-*d*₆) δ = 7.22 (br s, 1 H, overlapping with benzene-*d*₆), 6.64 (d, *J* = 7.0 Hz, 1 H), 5.98 (dd, *J* = 5.1, 7.0 Hz, 2 H), 1.72 (s, 3 H), 1.32 (br s, 18 H); MS(EI) *m/z* 469 [M]⁺, *m/z* 454 [M – Me]⁺, *m/z* 398 [M – NtBu]⁺.

Density-functional calculations were undertaken using a Linux cluster of IBM machines with Intel Xeon processors at the Westgrid facility at the University of British Columbia. The Gaussian'09 package was employed with the B3LYP functional.^{48,49} The LANL2DZ basis set with the corresponding ECP was used for the tungsten atoms; for all other atoms the 6-31G** basis set was used.^{50–56} The initial coordinates were imported from the solid-state molecular structures into GaussView and then freely refined as a neutral molecule and *S* = 0. The initial coordinates of the other geometric isomers were adjusted using GaussView and refined analogously. Single-point frequency calculations were undertaken to verify local minima. Both delta and lambda enantiomers were calculated for isomers of complexes **3**, **4**, and **5**. The use of dispersion correction was undertaken (using empirical dispersion = gd3bj).^{57,58} The dispersion correction was completed for the isomers of complexes **3** and **6**.

RESULTS AND DISCUSSION

Ligand Design. A series of bis(*tert*-butylimido)bis(*N,O*-chelate)tungsten complexes was prepared to probe characteristic *N,O*-chelate hemilability trends. The commercial availability of methyl-substituted pyridones and the modular synthesis of amide proligands allows for a variety of steric and electronic parameters to be easily evaluated (**3L–6L**, Scheme 2).³ The electronic properties of these proligands can be compared by considering their corresponding p*K*_a values. The electronic differences for proligands **3L** and **4L** are

expected to be minimal, and the value of unsubstituted pyridone (2-pyridone) with a p*K*_a of 17.0 (in DMSO) is used as a reference.⁵⁹ The p*K*_a's of **5L** and **6L** have not been reported. However, related alkyl ((Ph(H)NC(Me)O, 21.45) and aryl (Ph(H)NC(Ph)O, 18.77) amides have been reported (in DMSO).⁶⁰ The relative difference in p*K*_a between the two proligands **5L** and **6L** is expected to be similar. Notably this data shows that pyridones are more acidic by at least an order of magnitude than amides.

Although proligands **3L** and **4L** have similar electronic structures, they do have different substituent patterns. We propose that the variable placement of steric bulk affects hemilability (Figure 2). Notably proligand **3L** has bulk about

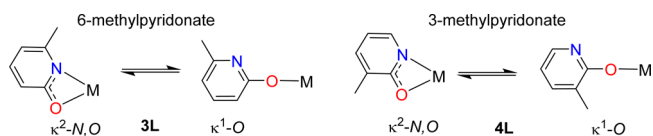


Figure 2. 6-Methylpyridonate (**3L**) κ^2 -*N,O* and κ^1 -*O* bonding modes (left) and 3-methylpyridonate (**4L**) κ^2 -*N,O* and κ^1 -*O* bonding modes (right). κ^1 -*O* demonstrates the aryloxyimine motif of pyridonate ligands.

the metal center in the κ^2 -*N,O* bonding mode, while in the κ^1 -*O* bonding mode the methyl group points away from the metal center (Figure 2). In contrast, in proligand **4L**, the methyl group points away from the metal center in the κ^2 -*N,O* bonding mode and points toward the metal center while in a κ^1 -*O* bonding mode (Figure 2). Indeed, the importance of the location of substituents has been noted in catalytic hydro-aminoalkylation³⁵ and is proposed to stem from differences in pyridonate hemilability. Another important feature of pyridonates is the aromatic system tied into the backbone of the NCO moiety, making the κ^1 -binding mode akin to aryloxy-type ligands (Figure 2).

Amides **5L** and **6L** have bulkier groups on the nitrogen (Figure 3) compared to pyridones **3L** and **4L**. While the



Figure 3. Amidate κ^2 -*N,O* and κ^1 -*O* bonding modes. **5L**, R¹ = Ph, R² = *t*Bu; **6L** R¹ = 2,6-diisopropylphenyl, R² = Ph.

increased steric demand of the amidates would offer substantial steric protection, the bulky substituents may also promote hemilability. Furthermore, for amidate ligands the κ^1 -*O* bonding mode can access two isomers, *E/Z* of the corresponding C=N double bond, demonstrating the further dynamic flexibility of these ligands (Figure 3). Comparing **5L** to the more sterically demanding **6L** allows for insights into how changing the steric parameters of 1,3-*N,O*-chelating ligands effects hemilability.

Tungsten Complex Synthesis and Characterization. The simplest synthetic strategy for installing 1,3-*N,O*-chelating ligands on high-valent early transition metals is through protonolysis reactions.^{34,38} Thus, protonolysis reactions of bis(*tert*-butylamido)bis(*tert*-butylimido)tungsten (**1**) with proligands **3L–6L** gave complexes **3–6**, respectively (Scheme 2).⁴¹ These new complexes can be isolated as analytically pure crystalline yellow solids in good yields ranging from 76% to

95%. Pyridonate complexes **3** and **4** are initially isolated as analytically pure viscous oils that crystallize over days. On the other hand, amidate complexes **5** and **6** are yellow solids which can be readily recrystallized from hexanes.

Of the possible coordination isomers (Figure 4) C_2 -symmetric *N-trans*, C_2 -symmetric *O-trans*, and C_1 isomers have all been observed for related bis(dimethylamido)bis(*N,O*-chelate)tungsten(IV) complexes.³⁴

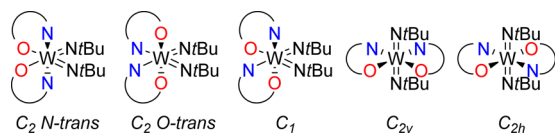


Figure 4. Possible stereoisomers of a bis(*N,O*-chelated)bis(*tert*-butylimido)tungsten complex. Simplified point groups assigned by ignoring the C_3 axis of *tert*-butyl groups.

Consistent with observations of group 4 complexes, the solid-state molecular structures for complexes **3–6** (Figure 5) are all six-coordinate complexes with two κ^2 -*N,O* bound 1,3-*N,O*-chelated ligands with either a pseudo- C_2 -symmetric *N-trans* or a pseudo- C_2 -symmetric *O-trans* coordination geometry (selected bond distances and angles are listed in Table 1).³⁴ These complexes exhibit a highly distorted octahedral geometry due to the acute bite angle of the 1,3-*N,O*-chelated ligands (58.41(7)–60.68(9)°). All *N,O*-chelated ligands have similar small O–W–N angles (Table 1) and are in agreement with the previously reported 1,3-*N,O*-chelating bite angles.^{34,61} The tungsten *tert*-butylimido (W–N) bond distances are also consistent throughout complexes **3–6** and range from 1.746(2) to 1.761(2) Å, which are elongated when compared to the starting material **1** (1.708(11) Å).⁶² This change in bond length is expected due to an increase in the coordination number.⁶² Similar to other reported 6-coordinate bis(*tert*-butylimido)tungsten(VI) complexes, the W–N–C imido bond angles approach linear bond angles and range from 151.0(2)° to 176.1(2)°.^{63–72} Complex **3** has a pseudo- C_2 -symmetric *O-trans* coordination environment of the 1,3-*N,O*-chelated ligands with shorter W1–O1 and W1–O2 bond lengths of 2.063(2) and 2.061(2) Å, respectively, and longer W1–N1 and W1–N2 bond lengths of 2.345(2) and 2.357(2) Å, respectively. This disparity in W–O versus W–N bond distances is indicative of an aryloxyimine bonding motif of the pyridonate ligand. This

assignment is further supported by the O1–C1 and O2–C7 bond lengths of 1.329(3) and 1.333(3) Å, respectively, indicating minimal multiple bond character between the oxygen and the carbon of the 6-methylpyridonate ligands in complex **3**.⁷³ Complexes **4**, **5**, and **6** exhibit a pseudo- C_2 -symmetric *N-trans* coordination environment in the solid state. The *N,O*-chelate contacts are consistent across the three complexes and range from 2.236(2) to 2.371(2) Å for the W–O bond lengths and from 2.094(2) to 2.140(3) Å for the W–N bond lengths. Complexes **4** and **5** have two inequivalent W–N–C imido bond angles in the solid state (176.1(2)°, 151.0(2)° and 175.0(2)°, 162.1(2)° respectively). Although these asymmetric *tert*-butylimido ligands are not observed in the solution phase by NMR spectroscopy, nonequivalent imido bond angles are commonly observed in the solid state and can often result from crystal packing.^{74,75} Among early transition metals, this is the first time that 1,3-*N,O*-chelates have been observed having substantially shorter M–N bonds over M–O bonds.^{35,38,61} This is attributed to the strong trans influence of *tert*-butylimido ligands.⁷⁶

Computational Investigations of Complex Geometries. Interestingly, the two pyridonate complexes, **3** and **4**, do not have the same geometric isomer in the solid state. To further investigate this switch in coordination environment for pyridonate complexes **3** and **4**, computational studies were undertaken to examine the relative energies of the different stereoisomers that these complexes can adopt. Density functional theory was employed using the B3LYP functional for optimization of stereoisomers, followed by a frequency calculation of each optimized isomer in order to compare the relative free energies of the stereoisomers.⁷⁷ Five possible isomers are shown in Figure 4; however, the C_{2v} and C_{2h} isomers are known to be highly disfavored as they have the two *tert*-butylimido ligands trans to each other; therefore, only the C_2 *N-trans*, C_2 *O-trans*, and C_1 isomers were considered.⁷⁸ Figure 6 shows the relative energies of the different isomers for complexes **3–5**. The computational modeling of complex **6** was complicated by the fact that only the C_2 *N-trans* isomer yields a six-coordinate bis(κ^2 -*N,O*-amidate) complex, while most other computed isomers produced five- or four-coordinate complexes with at least one amidate bound in a κ^1 -*O* fashion (see Supporting Information). The resulting energies of these four- or five-coordinate isomers are higher in energy than the C_2 *N-trans* complex.

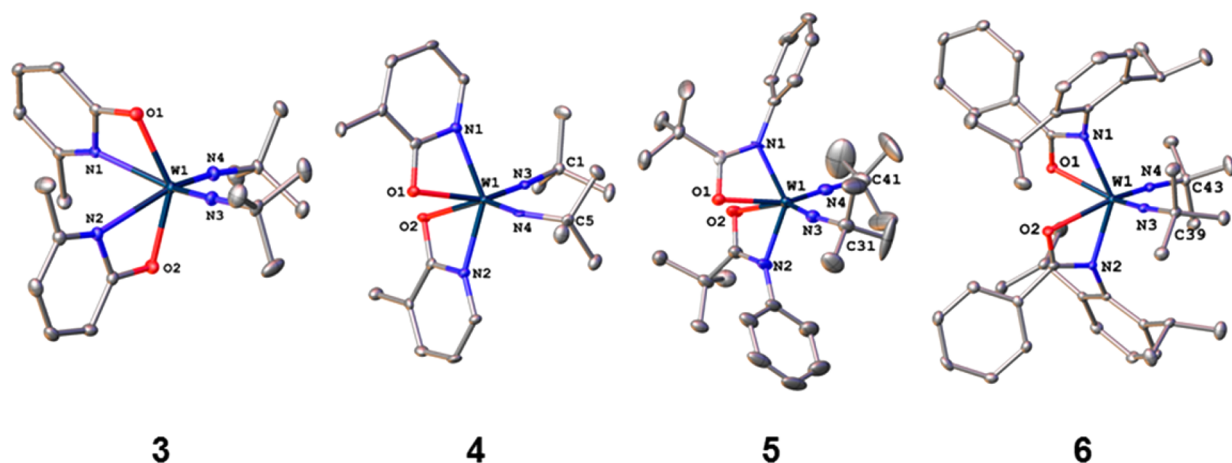


Figure 5. Solid-state molecular structures of complexes **3–6**, plotted at 50% ellipsoids, and hydrogen atoms are omitted for clarity.

Table 1. Selected Bond Distances and Angles for Complexes 3–6

3		4		5		6	
Selected Bond Distances (Å)							
W1–O1	2.063(2)	W1–O1	2.236(2)	W1–O1	2.24(1)	W1–O1	2.332(2)
W1–O2	2.061(2)	W1–O2	2.371(2)	W1–O2	2.339(2)	W1–O2	2.290(2)
W1–N1	2.345(2)	W1–N1	2.140(3)	W1–N1	2.02(3)	W1–N1	2.117(2)
W1–N2	2.357(2)	W1–N2	2.111(3)	W1–N2	2.094(2)	W1–N2	2.128(2)
W1–N3	1.759(2)	W1–N3	1.747(3)	W1–N3	1.752(2)	W1–N3	1.760(2)
W1–N4	1.751(2)	W1–N4	1.761(2)	W1–N4	1.746(2)	W1–N4	1.761(2)
Selected Bond Distances(deg)							
W1–N3–C13	165.4(2)	W1–N3–C1	176.1(2)	W1–N3–C31	162.1(2)	W1–N3–C39	171.2(2)
W1–N4–C17	167.2(2)	W1–N4–C5	151.0(2)	W1–N4–C41	175.0(2)	W1–N4–C43	170.8(2)
O1–W1–N1	59.84(8)	O1–W1–N1	60.68(9)	O1–W1–N1	59.8(9)	O1–W1–N1	58.73(6)
O2–W1–N2	59.67(8)	O2–W1–N2	58.91(9)	O2–W1–N2	58.41(7)	O2–W1–N2	59.14(6)

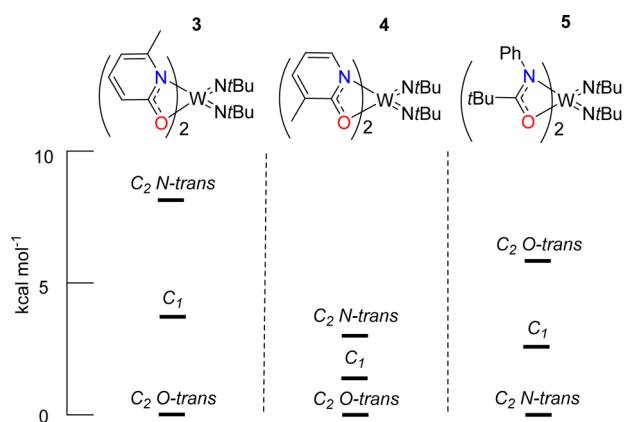
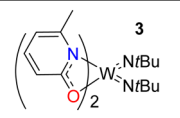
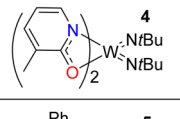
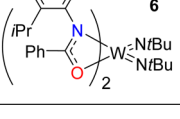


Figure 6. Relative free energies of C_2 *N-trans*, C_2 *O-trans*, and C_1 isomers of bis(*N,O*-chelate)bis(*tert*-butylimido)tungsten(VI) complexes; energies in kcal/mol, and each set of isomers is referenced to its corresponding lowest energy isomer.⁷⁹

The computational results predict that an *O-trans* coordination environment is the lowest free energy isomer for both pyridonate complexes 3 and 4. However, the model also predicts that the relative energy differences between the C_2 *O-trans*, C_1 , and C_2 *N-trans* isomers of complex 4 are small, and such similar energies may rationalize how crystal packing forces result in the observed (C_2 *N-trans*) structure for complex 4. Furthermore, the small energy difference between the calculated isomers suggested that facile access to multiple geometric isomers is possible, presuming that the barrier to isomerization is energetically feasible. Complexes 3 and 5 have coordination isomers with more pronounced energy differences between isomers, and in these cases the computationally predicted lowest energy isomer is consistent with the observed solid-state molecular structure. The findings of the computational results point out that steric demand of a 1,3-*N,O*-chelate influences how it is coordinated to the metal and suggests that when steric demand is removed multiple isomers may be accessible.

Solution-Phase Characterization Data. Room-temperature solution ^1H and ^{13}C NMR spectra for complexes 3–6 are consistent with C_2 -symmetric complexes in all cases (^1H NMR data summarized in Table 2); however, variable-temperature ^1H NMR experiments were recorded to probe whether fluxionality between geometric isomers could be observed. The observation of solution-phase hemilabile *N,O*-chelated ligands, such as κ^1 or bridging μ bonding modes, would lend support to their relevance in catalysis.

Table 2. Tabulated ^1H NMR Data Taken at 25 °C in Toluene- d_6 , 400 MHz

Complex	<i>t</i> -butylimido	<i>N,O</i> -chelate
	δ 1.44 (18H)	CH_3 δ 2.09 (6H); ArH δ 6.01 (2H), 6.18 (2H) and 6.93 (2H)
	δ 1.42 (18H)	CH_3 δ 1.92 (6H); ArH δ 6.07 (2H), 6.83 (2H) and 7.58 (2H)
	δ 1.14 (18H)	$\text{C}(\text{CH}_3)_3$ δ 1.14 (18H) (overlapping with $\text{NC}(\text{CH}_3)_3$); ArH δ 6.88 (2H), 7.04 (4H) and 7.24 (4H)
	δ 1.16 (18H)	$\text{CH}(\text{CH}_3)_2$ δ 0.90 (6H), 1.13 (6H), 1.43 (6H) and 1.68 (6H); CHCH_3 δ 3.87 (2H) and 4.10 (2H); ArH δ 6.84, 6.91 (2H), 7.18 (2H) and 7.68 (2H)

For 6-methylpyridonate complex 3 no changes were observed in the variable-temperature ^1H NMR spectrum from -30 to 90 °C. Only minor changes were observed from -40 to -80 °C. Two of the three aryl signals drift slightly from δ 6.93 and 6.01 at 25 °C to δ 6.68 and 5.76 at -80 °C, respectively. The temperature-shifted resonances are also broadened and suggest the dynamic formation of other isomers or aggregate species. However, due to the low abundance and broadened signals, no assignments can definitively be made. Due to the subtle changes in the variable-temperature ^1H NMR spectra, complex 3 is considered to be highly fluxional in solution.

The 3-methylpyridonate complex 4 also gives low-temperature spectra consistent with the fluxionality of the pyridonate ligands in solution. The resolution of three separate broadened pyridonate methyl resonances (δ 1.99, 1.87, and 1.85) as well as three separate *tert*-butylimido resonances (δ 1.58, 1.47, and 1.43) were observed at -70 °C, indicating that interconversion of the isomers above -70 °C is rapid. These observations cannot rule out the possibility of complex 4 adopting a bridging ligand motif or the formation of dimeric or aggregate species (vide infra).

For comparison, variable-temperature ^1H NMR experiments were also recorded for bis(amidate) complexes 5 and 6. The variable-temperature ^1H NMR spectra for complex 5 showed minimal changes from 25 to -80 °C; two aryl resonances at δ

7.24 and 7.04 broaden and migrate to δ 7.46 and 7.00, respectively. The only other changes in the low-temperature spectra were a new set of resonances, with low abundance, that emerged between -20 and -80 °C. The new resonances are broadened and are consistent with the dynamic formation of other isomers or aggregate species. Once again, no definitive assignments can be made.

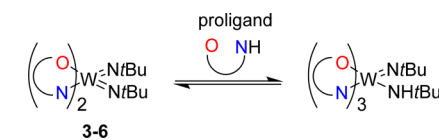
Finally, similar observations have been made for the bulky bis(amidate) complex 6. From 25 to 95 °C the isopropyl methyl and methine resonances broadened, suggesting that fluxionality is increased with increasing temperature. From 25 to -60 °C the spectra are consistent with a C_2 -symmetric complex.

The coordination modes in these complexes is not clearly demonstrated by ^1H NMR spectroscopy, and the data are best considered to be evidence that all complexes are fluxional in solution at catalytically relevant temperatures (>60 °C). Thus, we turned our attention to investigating the reactivity of complexes 3–6 in ligand exchange reactions and reactions with electrophiles to further probe N,O -chelate hemilability.

Reactivity Investigations. Ligand hemilability, resulting in the formation of an open coordination site, promotes ligand exchange reactions. To this end the 1:1 reaction of 3 and 4 in toluene- d_6 was monitored by ^1H NMR spectroscopy to probe if pyridonate ligand exchange between the complexes could be observed. Indeed, new *tert*-butylimido and methyl pyridonate signals appear at 1.41 and 1.87 in a 3:1 ratio, while the signals characteristic of 3 and 4 (see Table 2) were diminished in intensity. The aryl ^1H resonances also changed, consistent with the formation of a new bis(*tert*-butylimido)bis(N,O -chelate)-tungsten complex resulting from ligand exchange. This observation contrasts with the experiment treating 3 with amidate complex 5 under identical reaction conditions. In this case, no new resonances were observed by ^1H NMR spectroscopy. Furthermore, when complexes 5 and 6 were combined and monitored by ^1H NMR spectroscopy no new products were observed. These results show that pyridonate ligands undergo facile ligand exchange reactions, while amidate complexes are resistant to such ligand exchange reactions at ambient temperatures.

It has been shown that amido complexes can be accessed from imido complexes via protonation with a bulky alcohol or a Brønsted acid.^{41,46,47,69,80–82} The addition of 6-methylpyridonate complex 3 to 1 equiv of 3L (as a proton source) in toluene- d_6 resulted in no immediately observable reaction at 25 °C. However, variable-temperature ^1H NMR spectroscopy studies showed an equilibrium is present, and below -40 °C neither 3 nor 3L can be identified in solution. Below -40 °C multiple resonances are observed, indicating that the exchange of ligand with proligand is rapid and reversible. Although the low-temperature ^1H NMR spectrum of the reaction mixture was indicative of more than one single product, recrystallization of the resulting equilibrium mixture from hexanes at -30 °C resulted in precipitation of a mixture of amorphous solids and crystalline material found to be analytically pure tris(6-methylpyridonate)(*tert*-butylamido)(*tert*-butylimido)tungsten(VI) complex 7 (Table 3, entry 1). Electron impact mass spectrometry (EIMS) of the analytically pure solids showed a $[\text{M} - \text{HN}t\text{Bu}]^+$ ion, consistent with the molecular ion of tungsten with three pyridonate ligands and one *tert*-butylimido ligand. Single-crystal X-ray diffraction confirmed the formation of complex 7 (Figure 7). The solid-state molecular structure is evidence that 6-methylpyridone can protonate a *tert*-butylimido

Table 3. Reactivity of Complexes 3–6 with the Respective Proligands 3L–6L



entry	complex	proligand	product
1	3	3L	
2	4	4L	
3	5	5L	no reaction
4	6	6L	no reaction

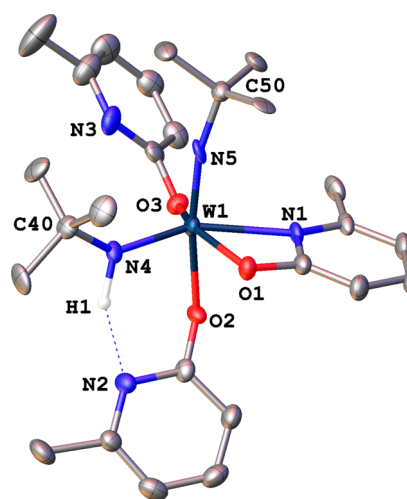
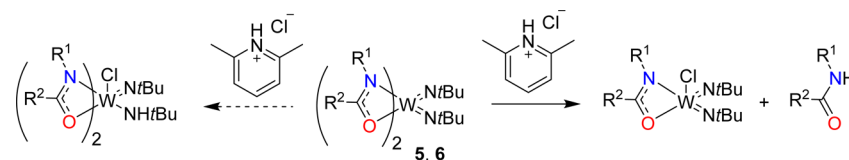


Figure 7. Solid-state molecular structure of complex 7, plotted at 50% ellipsoids with most hydrogen atoms omitted for clarity (except H1). Selected bond lengths (Angstroms): W1–O1 = 2.099(6), W1–O2 = 2.077(6), W1–O3 = 1.949(6), W1–N1 = 2.270(7), W1–N4 = 1.918(26), W1–N5 = 1.739(7). Selected bond angles (degrees): W1–N5–C50 = 166.7(6), W1–N4–C40 = 137.6(5), O1–W1–N1 = 60.6(2), N5–W1–O2 = 171.7(3), N1–W1–N5 = 91.5(3).

ligand, and notably this structure incorporates one κ^2 -pyridonate and two κ^1 -pyridonate ligands. The six-coordinate complex 7 has a distorted octahedral geometry in which the κ^2 - N,O 6-methylpyridonate adopts an aryloximine motif with a W1–O1 (2.099(5) Å) bond distance that is significantly shorter than the W1–N1 bond length (2.270(7) Å). The two κ^1 -O pyridonates have shorter tungsten oxygen bond lengths of 2.077(6) (W1–O2) and 1.949(6) (W1–O3) Å, which are consistent with previously reported bis(aryloxide)bis(imido)-tungsten(VI) complexes.⁸³ The *tert*-butylimido ligand has a short W1–N5 bond distance of 1.739(7) Å and a near linear W1–N5–C50 bond angle of 166.7(6)°, while the W1–N4 amido bond distance is 1.918(6) Å, with a W1–N4–C40 bond angle of 137.6(5)°. The hydrogen (H1) (located from residual

Scheme 3. Proposed Reaction of Lutidinium Hydrochloride with Bis(amidate) Complexes 5 and 6^a

^a(Left) Addition of HCl to tungsten complex, (right) protonolysis of the amidate ligand.

electron density) of the *tert*-butylamido ligand is oriented toward the nitrogen (N2) of the axial κ^1 -O pyridonate ligand indicative of hydrogen bonding, suggesting that the reversible protonation of the *tert*-butylimido substituent is assisted by the hemilabile pyridonate ligand.

The addition of 3-methylpyridonate complexes 4 and 4L was conducted in toluene-*d*₈, and the ¹H NMR spectrum of the mixture at 25 °C showed new broadened resonances in the alkyl and aryl regions, none of which correspond to proligand 4L, indicative of addition of the proligand to complex 4 forming a new tris(3-methylpyridonate)tungsten complex 8 (Table 3, entry 2). Variable-temperature ¹H NMR spectra show the broad resonances separate into multiple sharper resonances at lower temperatures, with the *tert*-butylimido singlet at 1.41 δ at 25 °C broadening into 6 singlets at -70 °C. Thus, this complex is fluxional at 25 °C. No solid-state molecular structures resulted from recrystallization attempts, and only amorphous solids were obtained. Similar to the mass spectrum of complex 7, EIMS experiments of the solids obtained yielded a molecular ion corresponding to tris(3-methylpyridonate)(*tert*-butylimido)tungsten [M - HN*t*Bu]⁺, supporting the formation of complex 8.

The reactivity of bis(amidate) complexes 5 and 6 was very different, whereby the addition of 1 equiv of 5L and 6L to complexes 5 and 6, respectively, showed no indication of a reaction as observed by ¹H NMR spectroscopy at various temperatures (from -40 to 90 °C). Furthermore, EIMS experiments conducted on the isolated solids of these reactions showed only the corresponding precursor bis(amidate)bis(*tert*-butylimido)tungsten complexes and proligands, with no evidence of a tris(amidate) product being formed.

These observations show that pyridonate complexes 3 and 4 have increased reactivity and can readily engage in proton shuttling, presumably due to reduced steric congestion and/or structural flexibility/hemilability compared to amidate ligands. Another contributing factor that may rationalize the lack of reactivity with 5L and 6L includes the lesser protic character of these amides. However, it should be noted that bulky tris(amidate) complexes of Ti(IV) are known.⁸⁴

To explore the effect of an alternative proton source, amidate complexes 5 and 6 were reacted with the Brønsted acid lutidinium hydrochloride (Scheme 3). In this case the lutidinium hydrochloride may result in protonation of the *tert*-butylimido ligand with addition of the chloride to the tungsten metal center or may protonate an amidate ligand.

The addition of lutidinium hydrochloride with amidate complex 5 was conducted at room temperature in toluene. Over a period of 2 h the poorly soluble lutidinium hydrochloride dissolved, and the reaction mixture was stirred for an additional 2 h. The ¹H NMR spectrum of the resulting crude material showed conversion of complex 5 to give three new singlet resonances in the aliphatic region. One *tert*-butyl resonance (1.01 ppm) was identified as proligand 5L. The

other two resonances at 1.26 and 0.92 ppm were assigned as two *tert*-butylimido ligands and the *tert*-butyl of the amidate (PhNC(*t*Bu)O⁻) ligand, respectively. These resonances were in a 2:1 ratio, suggesting the formation of a C_s-symmetric mono(*N*-phenylpivalamidate)bis(*tert*-butylimido)-chlorotungsten complex 9 (Scheme 3, right). Purification of 9 was challenging due to the presence of proligand 5L. However, single-crystal X-ray diffraction of colorless crystals formed from a concentrated hexanes solution confirmed the C_s-symmetric complex 9 (Figure 8).

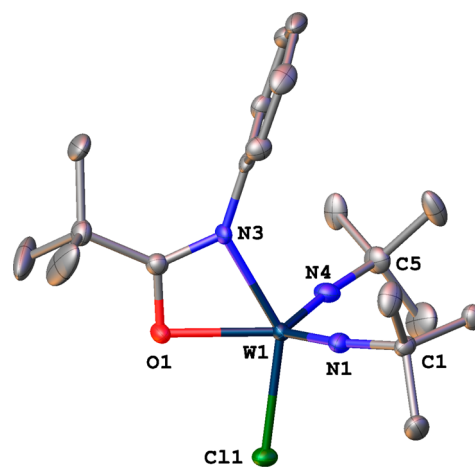


Figure 8. Solid-state molecular structure of complex 9, plotted at 50% ellipsoids and hydrogen atoms omitted for clarity. Selected bond lengths (Angstroms): W1–N1 = 1.744(2), W1–N2 = 1.737(3), W1–N3 = 2.120(3), W1–O1 = 2.166(3), W1–Cl1 = 2.3573(8). Selected bond angles (degrees): W1–N1–C1 = 163.2(2), W1–N2–C5 = 170.1(3), O1–W1–N1 = 122.3(1), O1–W1–N2 = 123.3(1), N3–W1–Cl1 = 143.96(7), O1–W1–N3 = 60.11(9).

Complex 9 exhibits a distorted trigonal bipyramidal coordination geometry.⁷⁷ The amidate is symmetrically bound with the W–N bond (2.120(3) Å) being shorter than the W–O bond (2.166(3) Å). Notably, W–O has shortened significantly when compared to the W–O bonds in precursor 5 (2.24(1) and 2.339(2) Å). The W–N bonds of the *tert*-butylimido ligands in complex 9 are 1.744(2) and 1.737(3) Å for W1–N1 and W1–N2 respectively, which are also shorter compared to those of 5. The overall shortening of tungsten ligand bonds is attributed to a reduced coordination number from 6 to 5 and incorporation of a chloride ligand. The W1–Cl1 bond length of 2.3573(8) Å is consistent with a reported isostructural bis(*tert*-butylimido)chloro(guanidinate)tungsten complex.⁶⁵ Variable-temperature ¹H NMR spectroscopy of the reaction mixture up to 95 °C and down to -40 °C showed no equilibrium between proligand 5L and complex 9; however, the amidate resonances shift slightly with temperature (see Supporting Information). At temperatures below -40 °C

proligand **5L** precipitates out of the toluene- d_8 solution. Throughout there was no spectral evidence suggesting that a bis(amidate)(*tert*-butylamido)chloro(*tert*-butylimido)tungsten complex was formed; rather, we propose that the lutidinium hydrochloride protonates the sterically demanding and hemilabile amidate ligand and forms complex **9** via elimination of proligand **5L**. Alternatively, the lutidinium hydrochloride could protonate an imido ligand of complex **9**, followed by an N–H activation by a coordinated amidate forming proligand **5L** and complex **9**.

A minor product of the reaction was shown to be a (*tert*-butylamido)(*tert*-butylimido)dichloro(*N*-phenylpivalamidate)-tungsten(VI) complex (**10**) by single-crystal X-ray diffraction (Figure 9). Isolation of analytically pure complex **10** was not

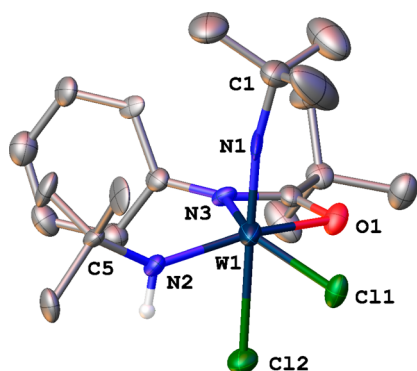
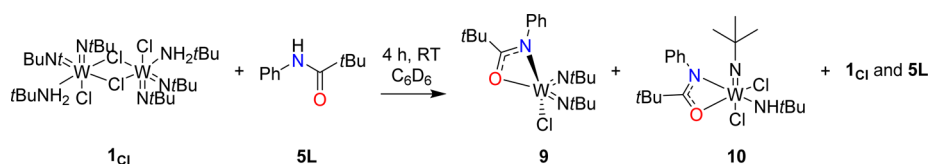


Figure 9. Solid-state molecular structure of complex **10**, plotted at 50% ellipsoids with most hydrogen atoms omitted for clarity. Selected bond lengths (Angstroms): W1–N1 = 1.741(10), W1–N2 = 2.014(19), W1–N3 = 1.89(2), W1–O1 = 2.00(2), W1–C11 = 2.502(9), W1–C1 = 2.480(3). Selected bond angles (degrees): W1–N1–C1 = 170(1), W1–N2–C5 = 141(2), O1–W1–N3 = 66.6(9).

accessible; like complex **9** purification of **10** was hindered by proligand (**5L**) contamination. In order to discern the reactivity pathway we added a dimeric (*tert*-butylamine)bis(*tert*-butylimido)dichlorotungsten complex (**1_{Cl}**) to 1 equiv of proligand **5L** in an NMR tube (Scheme 4).⁸⁵ Unexpectedly, the major product of the reaction was the monochloride amidate complex **9**, accompanied by unreacted **5L** and **1_{Cl}** as well as small amounts of complex **10** (Scheme 4). It should be noted that reactions involving exchanges of tungsten imido, amido, amine, and chloride ligands have been observed before on similar systems bearing *tert*-butoxide ligands. These examples were also reported to be difficult to characterize.⁸⁶ Interestingly, the major product (complex **9**, Scheme 4) prefers two *tert*-butylimido ligands rather than a mixed imido/amido/amine complex as observed in the tungsten *tert*-butoxide complexes. A plausible explanation for this is that the amidate ligands provide increased steric demand versus a *tert*-butoxide ligand, resulting in complex **9** as the preferred amidate product.

Scheme 4. Reaction of Complex **1_{Cl}** with Proligand **5L**^a



^aThe reaction was conducted in benzene- d_6 in an NMR tube with a resealable cap.

Interestingly, the addition of lutidinium hydrochloride to amidate complex **6** did not proceed analogous to that of **5** when conducted at room temperature in toluene. The crude reaction mixture of lutidinium hydrochloride and amidate complex **6** showed largely unreacted **6** (~90%), and upon work up only unreacted complex **6** could be reisolated in reduced yields by trituration with hexanes. The reduced reactivity of complex **6** with lutidinium hydrochloride can be attributed to the sterically demanding 2,6-diisopropylphenyl groups on the amidate ligands.

Pyridonate complexes **3** and **4** were also treated with lutidinium hydrochloride. When 6-methylpyridonate complex **3** was added to 1 equiv of lutidinium hydrochloride for 4 h in toluene, a red orange solid formed upon removal of volatiles. The ¹H NMR spectrum of the crude material suggested that one major product is formed along with unreacted **3**. A single crystal was obtained by slow evaporation of a concentrated benzene solution of the product. This product was shown to be chloro(*tert*-butylimido)((κ^1 -O)6-methylpyridonate)bis((κ^2 -*N,O*)6-methylpyridonate)tungsten(VI) (**11**). The solid-state molecular structure of **11** is shown in Figure 10. The

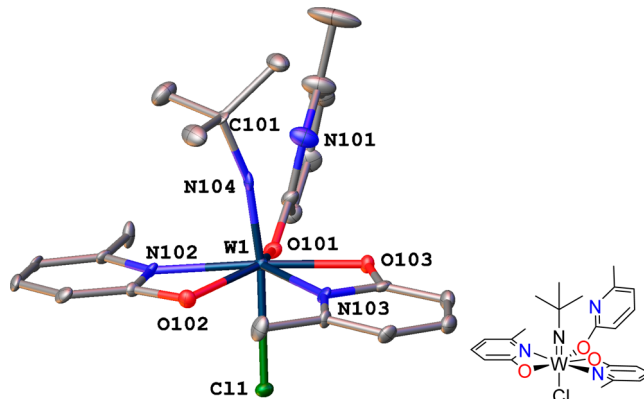


Figure 10. Solid-state molecular structure of complex **11**, plotted at 50% ellipsoids and hydrogen atoms omitted for clarity. Selected bond lengths (Angstroms): W1–N102 = 2.227(9), W1–N103 = 2.22(1), W1–N104 = 1.724(8), W1–O101 = 1.938(6), W1–O102 = 2.103(6), W1–O103 = 2.085(6), W1–C11 = 2.498(2). Selected bond angles (degrees): W1–N104–C101 = 165.8(8), N104–W1–C11 = 171.3(2).

coordination geometry of the complex can be described as a distorted pentagonal bipyramid, where each tungsten-bound atom occupies one site. The κ^2 -*N,O* pyridonate ligands exhibit an aryloxyimine bonding motif as evidenced by the shorter W–O bond lengths (W1–O102, 2.103(6) Å; W1–O103, 2.085(6) Å) versus the longer W–N bond lengths (W1–N102, 2.227(9) Å; W1–N103, 2.22(1) Å). The κ^1 -O pyridonate in **11** is analogous to that of complex **7**. The chlorido ligand is trans to the *tert*-butylimido ligand and exhibits an elongated W–Cl bond length (W1–Cl1, 2.498(2) Å).⁸⁷ The *tert*-butylimido

ligand has a W–N4 bond length of 1.724(8) Å and a W–N104–C101 bond angle of 165.8(8)°.

Complex 11 is thought to form via ligand redistribution resulting from protonation of a tungsten *tert*-butylimido group to release free *tert*-butylamine. Interestingly, complex 11 is C_3 symmetric in solution phase, as observed in the ^1H NMR spectrum at 25 °C. Two broad singlets of equal integration are observed at δ 2.53 and 1.07, which are attributed to the pyridonate methyl and the *tert*-butylimido groups, respectively. The observed broad resonances and observed C_3 symmetry are attributed to hemilability and fluxionality in the pyridonate ligands. The ^1H NMR spectrum of the crude solids isolated from the reaction shows unreacted 3 and one major product which has been assigned to be 11 along with a minor product proposed to be (bis(*tert*-butylimido)chloro(6-methylpyridonate)tungsten(VI)) complex 12. To verify this formulation, 12 has been synthesized independently by treatment of 3 with trimethylsilyl chloride (TMSCl). One equivalent or excess TMSCl can be reacted with pyridonate complex 3 at 60 °C overnight. Removal of the volatiles under vacuum yields dark orange solids. After recrystallization from warm hexanes at –30 °C, crystals suitable for X-ray diffraction could be obtained, and the solid-state molecular structure is shown in Figure 11. Complex 12 is isostructural to 9 and has

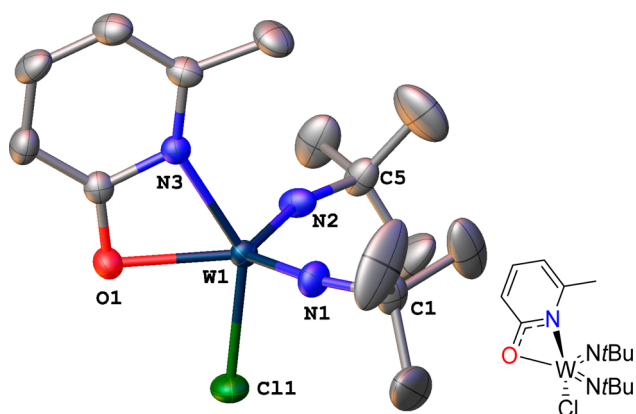


Figure 11. Solid-state molecular structure of complex 12, plotted at 50% ellipsoids with hydrogen atoms omitted for clarity. Selected bond lengths (Angstroms): W1–N1 = 1.744(4), W1–N2 = 1.747(3), W1–N3 = 2.135(4), W1–O1 = 2.146(3), W1–Cl1 = 2.346(1). Selected bond angles (degrees): W1–N1–C1 = 161.6(3), W1–N2–C5 = 163.8(3), O1–W1–N1 = 123.0(1), O1–W1–N2 = 125.3(1), N3–W1–Cl1 = 144.5(1), O1–W1–N3 = 61.3(1).

nearly identical bond metrics for the tungsten ligand contacts (Figures 8 and 10).⁸⁸ The solution-phase ^1H NMR spectrum of complex 12 exhibits broad resonances for the *tert*-butylimido and pyridonate methyl signals at δ 1.31 and 1.97, respectively, in a 6:1 ratio. These ^1H NMR resonances match that of the proposed minor product resulting from the reaction with lutidinium hydrochloride and complex 3.

The addition of 3-methylpyridonate complex 4 with 1 equiv of lutidinium hydrochloride at room temperature for 4 h yields a pale white solid. The ^1H NMR spectrum of the crude reaction mixture shows resonances corresponding to 4 and two other products which correspond to the 3-methylpyridonate-bridged di((3-methylpyridonate)bis(*tert*-butylimido)chlorotungsten) complex 13 and an unknown impurity 14. Attempts to isolate complexes 13 and 14 from the reaction mixture have not been met with success. However, complex 13 was independently synthesized via treatment of 4 with TMSCl. In the solid-state complex 13 exhibits a dimeric structure (Figure 12; selected bond distances and angles are listed in Table 4). The nearly C_2 -symmetric complex has two μ^2 -*N,O*-3-methylpyridonate ligands that bridge between two bis(*tert*-butylimido)chlorotungsten fragments. The W1–W2 distance is 3.958(8) Å, which is well beyond the sum of the covalent radii (3.34 Å),³⁹ indicating that there is no bonding interaction between tungsten metal centers. Each tungsten metal center contains two *tert*-butylimido ligands, one chloride, one μ -*N*-3-methylpyridonate, and one μ -*O*-3-methylpyridonate. The 5-coordinate tungsten metal centers are best described as distorted square pyramidal, with τ values of 0.14 and 0.16 for W1 and W2, respectively.⁸⁹

In sharp contrast, amidate complexes 5 and 6 did not react with the bulky TMSCl reagent under the same conditions. In these cases the unreacted amidate complexes 5 and 6 could be recovered after the reaction.

These results demonstrate the increased reactivity of pyridonate complexes 3 and 4 to that of amidate complexes 5 and 6. Both pyridonate complexes 3 and 4 and amidate complexes 5 and 6 are saturated six-coordinate complexes in the solid state and have solution-phase ^1H NMR spectra, suggesting that the 1,3-*N,O*-chelated tungsten complexes behave similarly. However, the strikingly different reactivity patterns of these two classes of complexes clearly demonstrate that pyridonate ligands have diverse reactivity manifolds accessible in comparison to their amidate counterparts. We propose that the increased ability of the pyridonate ligands to undergo ligand exchange reactions stems from their enhanced hemilability. Furthermore, pyridonate ligands were shown to

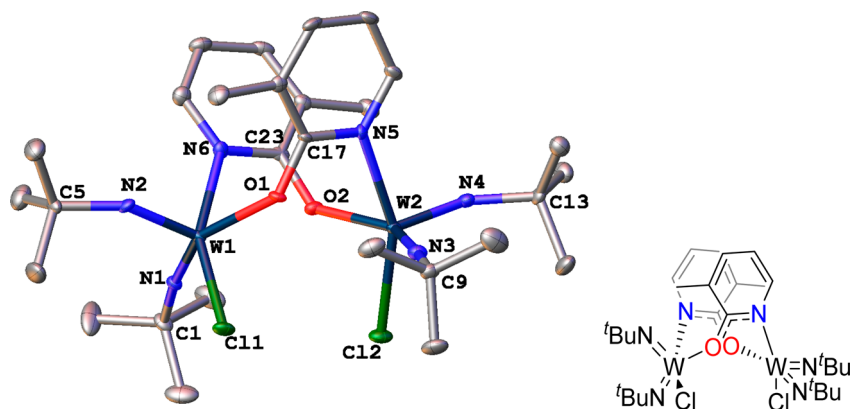


Figure 12. Solid-state molecular structure of complex 13, plotted at 50% ellipsoids with hydrogen atoms omitted for clarity.

Table 4. Bond Distances and Bond Angles of Complex 13

bond distances (Å)				bond angles (deg)			
W1–O1	2.107(3)	W2–O2	2.122(3)	W1–N1–C1	172.4(3)	W2–N3–C9	173.7(3)
W1–N6	2.171(3)	W2–N5	2.166(3)	W1–N2–C5	150.2(3)	W2–N4–C13	146.4(3)
W1–N2	1.753(4)	W2–N4	1.754(3)	N6–W1–C11	155.45(9)	N5–W2–C12	156.09(9)
W1–N1	1.736(4)	W2–N3	1.735(3)	O1–W1–N6	80.1(1)	O2–W2–N5	79.1(1)
W1–C11	2.379(1)	W2–C12	2.386(1)	O1–W1–N2	105.6(1)	O2–W2–N4	107.5(1)
O1–C17	1.319(4)	O2–C23	1.307(5)	O1–W1–N1	146.9(1)	O2–W2–N3	146.3(1)
N5–C17	1.338(5)	N6–C23	1.345(5)	O1–W1–N1	146.9(1)	O2–W2–N3	146.3(1)
W1–O2	2.872(3)	W2–O1	2.794(3)	N2–W1–N1	107.3(2)	N4–W2–N3	105.8(2)

adopt bridging interactions which may promote the observed ligand redistribution reactions. No κ^1 -O bonding modes have been observed in this study for any amidate ligands. Furthermore, no tungsten amidate complexes were shown to have a coordination number above 6, in contrast to pyridonate complexes. This mirrors past reports of titanium amidate and pyridonate complexes, where 7-coordinate tris(pyridonate) complexes have been disclosed, while the coordination numbers of titanium amidate complexes has not exceeded 6 for monometallic species.³

CONCLUSION

The new bis(*tert*-butylimido)bis(*N,O*-chelate)tungsten complexes 3–6 were synthesized by simple and high-yielding protonolysis reactions. Variable-temperature ¹H NMR spectroscopic experiments and computational modeling of the different coordination isomers suggest that the 1,3-*N,O*-chelates display fluxional character. The reactivity investigations concluded that pyridonate ligands exhibit a broader scope of coordination modes and hence reactivity than amidate ligands; this is attributed to the increased hemilability of the pyridonate ligands. The electronic difference between the pyridonate and the amidate ligands is in part responsible for the increase in hemilability, with the pyridonate ligand exhibiting more diverse bonding modes, such as the aryloxyimine motif and bridging bonding modes. Notably pyridonate ligands provide reduced steric protection at the metal center, and this also promotes enhanced reactivity. These results point toward the benefits of using pyridonate ligands when κ^1 -species are invoked as key reactive intermediates in catalytic cycles where the metal–ligand cooperative effects could be used to advantage. Most importantly, pyridonate ligands have been shown to engage in hydrogen bonding interactions with metal amido ligands, suggesting that pyridonate ligands can be used to advantage in reactions where proton shuttling is required. An example of which is the Cp*Ir(III) pyridonate catalysts for ligand-assisted dehydrogenation of alcohols.^{10,11} Here we also show that pyridonate complexes can readily form dimeric species, a feature that has been used to advantage in the development of our bis(pyridonate)Ti catalyst for chemoselective intramolecular hydroaminoalkylation.³⁵ In contrast, the increased robustness of amidate complexes points toward their preferential application in catalytic reactions where ligand loss or the formation of dimers or aggregate species is postulated to result in catalyst degradation. These observations rationalize why our bulky bis(amidate)Ti complex is an optimized catalyst for hydroamination, a reaction in which bridging imido dimers is known to result in catalyst death.^{11,90} Further studies focus on the development of new complexes and catalysts that use these reactivity trends to advantage for E–H bond activations while avoiding complex or catalyst decomposition.

ASSOCIATED CONTENT

Supporting Information

The Supporting Information is available free of charge on the ACS Publications website at DOI: 10.1021/acs.inorgchem.6b02959.

Crystallographic information, crystallographic parameters, asymmetric unit for the solid-state molecular structure of complex 3–7 and 9–13, discussion of solid-state molecular structure of complexes 9 and 12, solid-state molecular structure of 9 and 13, overlay of solid-state structures of 9 and 12, density functional theory calculations, computed isomers of complexes 3–5 and relative energies, images of computed isomers of complexes 3–6, overlay of DFT-computed and solid-state molecular structure of complexes 3–6, NMR spectra of complexes 3–13, references (PDF) Computational.xyz files (PDF) CIF files and crystallographic data (TXT)

AUTHOR INFORMATION

Corresponding Author

*E-mail: schafer@chem.ubc.ca.

ORCID

Laurel L. Schafer: 0000-0003-0354-2377

Notes

The authors declare no competing financial interest.

ACKNOWLEDGMENTS

The authors thank NSERC and UBC for financial support. J.M.C. thanks Dr. Jacky Yim, Mr. Scott Ryken, and Mr. Damon Gilmour for collection of X-ray data sets and Dr. Brian Patrick for assistance with twinned and/or highly disordered structures. J.M.C. thanks Dr. Jean Michel Lauzon for assistance with DFT calculations. L.L.S. and J.M.C. thank the reviewers for helpful comments and suggestions. This work was undertaken, in part, thanks to funding from the Canada Research Chairs program (LLS).

REFERENCES

- Jeffrey, J. C.; Rauchfuss, T. B. Metal complexes of hemilabile ligands. Reactivity and structure of dichlorobis(o-(diphenylphosphino)anisole)ruthenium(II). *Inorg. Chem.* **1979**, *18*, 2658–2666.
- Slone, C. S.; Weinberger, D. A.; Mirkin, C. A. The Transition Metal Coordination Chemistry of Hemilabile Ligands. *Progress in Inorganic Chemistry*; John Wiley & Sons, Inc., 2007; pp 233–350.
- Ryken, S. A.; Schafer, L. L. *N,O*-Chelating Four-Membered Metallacyclic Titanium(IV) Complexes for Atom-Economic Catalytic Reactions. *Acc. Chem. Res.* **2015**, *48*, 2576–2586.

- (4) Drover, M. W.; Schafer, L. L.; Love, J. A. Capturing HBCy₂: Using N,O-Chelated Complexes of Rhodium(I) and Iridium(I) for Chemoselective Hydroboration. *Angew. Chem., Int. Ed.* **2016**, *55*, 3181–3186.
- (5) Drover, M. W.; Schafer, L. L.; Love, J. A. 1,3-N,O-Complexes of Late Transition Metals. Ligands with Flexible Bonding Modes and Reaction Profiles. *J. Am. Chem. Soc.* **2016**, *138*, 8396.
- (6) Lee, A. V.; Schafer, L. L. Modular N,O-Chelating Ligands: Group-4 Amidate Complexes for Catalytic Hydroamination. *Eur. J. Inorg. Chem.* **2007**, *2007*, 2245–2255.
- (7) Haehnel, M.; Yim, J. C. H.; Schafer, L. L.; Rosenthal, U. Facile Access to Tuneable Schwartz's Reagents: Oxidative Addition Products from the Reaction of Amide N-H Bonds with Reduced Zirconocene Complexes. *Angew. Chem., Int. Ed.* **2013**, *52*, 11415–11419.
- (8) Drover, M. W.; Schafer, L. L.; Love, J. A. Amidate-Ligated Complexes of Rhodium(I): A Showcase of Coordination Flexibility. *Organometallics* **2015**, *34*, 1783–1786.
- (9) Flood, T. C.; Lim, J. K.; Deming, M. A. Generation of Coordinative Unsaturation at Osmium via Ring-Opening Equilibration of a 2-Pyridonato Chelate Complex. *Organometallics* **2000**, *19*, 2310–2317.
- (10) Fujita, K.-i.; Tanino, N.; Yamaguchi, R. Ligand-Promoted Dehydrogenation of Alcohols Catalyzed by Cp*Ir Complexes. A New Catalytic System for Oxidant-Free Oxidation of Alcohols. *Org. Lett.* **2007**, *9*, 109–111.
- (11) Royer, A. M.; Rauchfuss, T. B.; Gray, D. L. Organoiridium Pyridonates and Their Role in the Dehydrogenation of Alcohols. *Organometallics* **2010**, *29*, 6763–6768.
- (12) Hill, J. E.; Profflet, R. D.; Fanwick, P. E.; Rothwell, I. P. Synthesis, Structure, and Reactivity of Aryloxo(imido)titanium Complexes. *Angew. Chem., Int. Ed. Engl.* **1990**, *29*, 664–665.
- (13) Walsh, P. J.; Baranger, A. M.; Bergman, R. G. Stoichiometric and catalytic hydroamination of alkynes and allene by zirconium bisamides Cp₂Zr(NHR)₂. *J. Am. Chem. Soc.* **1992**, *114*, 1708–1719.
- (14) Shi, Y.; Ciszewski, J. T.; Odom, A. L. Ti(NMe₂)₄ as a Precatalyst for Hydroamination of Alkynes with Primary Amines. *Organometallics* **2001**, *20*, 3967–3969.
- (15) Pohlki, F.; Doye, S. The Mechanism of the [Cp₂TiMe₂]-Catalyzed Intermolecular Hydroamination of Alkynes. *Angew. Chem., Int. Ed.* **2001**, *40*, 2305–2308.
- (16) Zhang, Z.; Schafer, L. L. Anti-Markovnikov Intermolecular Hydroamination: A Bis(amidate) Titanium Precatalyst for the Preparation of Reactive Aldimines. *Org. Lett.* **2003**, *5*, 4733–4736.
- (17) Gribkov, D. V.; Hultzsck, K. C. Hydroamination/Cyclization of Aminoalkenes Using Cationic Zirconocene and Titanocene Catalysts. *Angew. Chem., Int. Ed.* **2004**, *43*, 5542–5546.
- (18) Leitch, D. C.; Payne, P. R.; Dunbar, C. R.; Schafer, L. L. Broadening the Scope of Group 4 Hydroamination Catalysis Using a Tethered Ureate Ligand. *J. Am. Chem. Soc.* **2009**, *131*, 18246–18247.
- (19) Ryken, S. A.; Payne, P. R.; Schafer, L. L. Tight Bite Angle N,O-Chelates. Amidates, Ureates and Beyond. *Ligand Design in Metal Chemistry*; John Wiley & Sons, Ltd., 2016; pp 364–405.
- (20) Manna, K.; Eedugurala, N.; Sadow, A. D. Zirconium-Catalyzed Desymmetrization of Aminodialkenes and Aminodialkynes through Enantioselective Hydroamination. *J. Am. Chem. Soc.* **2015**, *137*, 425–435.
- (21) Clerici, M. G.; Maspero, F. Catalytic C-Alkylation of Secondary Amines with Alkenes. *Synthesis* **1980**, *1980*, 305–306.
- (22) Nugent, W. A.; Ovenall, D. W.; Holmes, S. J. Catalytic C-H activation in early transition-metal dialkylamides and alkoxides. *Organometallics* **1983**, *2*, 161–162.
- (23) Herzon, S. B.; Hartwig, J. F. Direct, Catalytic Hydroaminoalkylation of Unactivated Olefins with N-Alkyl Arylamines. *J. Am. Chem. Soc.* **2007**, *129*, 6690–6691.
- (24) Bexrud, J. A.; Eisenberger, P.; Leitch, D. C.; Payne, P. R.; Schafer, L. L. Selective C–H Activation α to Primary Amines. Bridging Metallaaziridines for Catalytic, Intermolecular α -Alkylation. *J. Am. Chem. Soc.* **2009**, *131*, 2116–2118.
- (25) Eisenberger, P.; Ayinla, R. O.; Lauzon, J. M. P.; Schafer, L. L. Tantalum–Amidate Complexes for the Hydroaminoalkylation of Secondary Amines: Enhanced Substrate Scope and Enantioselective Chiral Amine Synthesis. *Angew. Chem., Int. Ed.* **2009**, *48*, 8361–8365.
- (26) Garcia, P.; Lau, Y. Y.; Perry, M. R.; Schafer, L. L. Phosphoramidate Tantalum Complexes for Room-Temperature C-H Functionalization: Hydroaminoalkylation Catalysis. *Angew. Chem., Int. Ed.* **2013**, *52*, 9144–9148.
- (27) Severin, R.; Doye, S. The catalytic hydroamination of alkynes. *Chem. Soc. Rev.* **2007**, *36*, 1407–1420.
- (28) Huang, L.; Arndt, M.; Gooßen, K.; Heydt, H.; Gooßen, L. J. Late Transition Metal-Catalyzed Hydroamination and Hydroamidation. *Chem. Rev.* **2015**, *115*, 2596–2697.
- (29) Chong, E.; Garcia, P.; Schafer, L. L. Hydroaminoalkylation: early-transition-metal-catalyzed α -alkylation of amines. *Synthesis* **2014**, *46*, 2884–2896.
- (30) Lawrence, S. A. *Amines: Synthesis, Properties and Applications*; Cambridge University Press, U.K., 2006.
- (31) Yim, J. C. H.; Bexrud, J. A.; Ayinla, R. O.; Leitch, D. C.; Schafer, L. L. Bis(amidate)bis(amido) Titanium Complex: A Regioselective Intermolecular Alkyne Hydroamination Catalyst. *J. Org. Chem.* **2014**, *79*, 2015–2028.
- (32) Lui, E. K. J.; Schafer, L. L. Facile Synthesis and Isolation of Secondary Amines via a Sequential Titanium(IV)-Catalyzed Hydroamination and Palladium-Catalyzed Hydrogenation. *Adv. Synth. Catal.* **2016**, *358*, 713–718.
- (33) Yim, J. C. H.; Schafer, L. L. Efficient Anti-Markovnikov-Selective Catalysts for Intermolecular Alkyne Hydroamination: Recent Advances and Synthetic Applications. *Eur. J. Org. Chem.* **2014**, *2014*, 6825–6840.
- (34) Thomson, R. K.; Zahariev, F. E.; Zhang, Z.; Patrick, B. O.; Wang, Y. A.; Schafer, L. L. Structure, Bonding, and Reactivity of Ti and Zr Amidate Complexes: DFT and X-Ray Crystallographic Studies. *Inorg. Chem.* **2005**, *44*, 8680–8689.
- (35) Chong, E.; Schafer, L. L. 2-Pyridonate Titanium Complexes for Chemoselectivity. Accessing Intramolecular Hydroaminoalkylation over Hydroamination. *Org. Lett.* **2013**, *15*, 6002–6005.
- (36) Chong, E.; Brandt, J. W.; Schafer, L. L. 2-Pyridonate Tantalum Complexes for the Intermolecular Hydroaminoalkylation of Sterically Demanding Alkenes. *J. Am. Chem. Soc.* **2014**, *136*, 10898–10901.
- (37) Boyle, T. J.; Sivonxay, E. Synthesis and characterization of 2-hydroxy-pyridine modified Group 4 alkoxides. *J. Coord. Chem.* **2016**, *69*, 1419–1438.
- (38) Bexrud, J. A.; Schafer, L. L. Zirconium bis(pyridonate): a modified amidate complex for enhanced substrate scope in aminoalkene cyclohydroamination. *Dalton Trans.* **2010**, *39*, 361–363.
- (39) Cordero, B.; Gomez, V.; Platero-Prats, A. E.; Reves, M.; Echeverria, J.; Cremades, E.; Barragan, F.; Alvarez, S. Covalent radii revisited. *Dalton Trans.* **2008**, 2832–2838.
- (40) Pyykkö, P.; Atsumi, M. Molecular Single-Bond Covalent Radii for Elements 1–118. *Chem. - Eur. J.* **2009**, *15*, 186–197.
- (41) Takacs, J.; Cavell, R. G. Synthesis and Characterization of New d₀ Tungsten and Molybdenum Imido Complexes with Heteroatomic Bifunctional O-N Chelate Ligands. *Inorg. Chem.* **1994**, *33*, 2635–2638.
- (42) Weiss, K.; Schubert, U.; Schrock, R. R. Investigations of polymerizations and metathesis reactions. 6. Metathesis-like reaction of a tungsten alkylidene complex with cyclohexyl isocyanate. *Organometallics* **1986**, *5*, 397–398.
- (43) Yeh, W. Y.; Peng, S. M.; Liu, L. K. W(η^4 -C₄Ph₄)(η^4 -C₄Ph₄H)(η^2 -CH₃C(O)NH): a compound containing $\eta^2(3e)$ -acetamido, $\eta^4(4e)$ -cyclobutadiene, and $\eta^4(5e)$ -butadienyl ligands. *Inorg. Chem.* **1993**, *32*, 2965–2967.
- (44) Minato, M.; Sakai, H.; Weng, Z.-G.; Zhou, D.-Y.; Kurishima, S.; Ito, T.; Yamasaki, M.; Shiro, M.; Tanaka, M.; Osakada, K. Syntheses, Structures, and Reactions of η^2 -N-Acylamido-N,O Hydrido Complexes of Molybdenum(II) and Tungsten(II). *Organometallics* **1996**, *15*, 4863–4871.
- (45) Barnett, N. D. R.; Massey, S. T.; McGowan, P. C.; Wild, J. J.; Abboud, K. A.; McElwee-White, L. Oxidation of the Zwitterion

- (CO)₅WPhNPhC(OMe)Ph with I₂. Formation of Tungsten(IV) Imido Complexes and a Tungsten(VI) Metallacycle. *Organometallics* **1996**, *15*, 424–428.
- (46) Lam, H.-W.; Wilkinson, G.; Hussain-Bates, B.; Hursthouse, M. B. Reactions of tert-butyl isocyanate and trimethylsilyl azide with imidoamido compounds of chromium, molybdenum and tungsten. *J. Chem. Soc., Dalton Trans.* **1993**, 781–788.
- (47) Nugent, W. A.; Harlow, R. L. Some bis(tert-butylimido) complexes of the Group 6 transition metals and a related alkylamido derivative. *Inorg. Chem.* **1980**, *19*, 777–779.
- (48) Becke, A. D. Density-functional thermochemistry. III. The role of exact exchange. *J. Chem. Phys.* **1993**, *98*, 5648–5652.
- (49) Frisch, M. J.; Trucks, G. W.; Schlegel, H. B.; Scuseria, G. E.; Robb, M. A.; Cheeseman, J. R.; Scalmani, G.; Barone, V.; Mennucci, B.; Petersson, G. A.; Nakatsuji, H.; Caricato, M.; Li, X.; Hratchian, H. P.; Izmaylov, A. F.; Bloino, J.; Zheng, G.; Sonnenberg, J. L.; Hada, M.; Ehara, M.; Toyota, K.; Fukuda, R.; Hasegawa, J.; Ishida, M.; Nakajima, T.; Honda, Y.; Kitao, O.; Nakai, H.; Vreven, T.; Montgomery, J. A., Jr.; Peralta, J. E.; Ogliaro, F.; Bearpark, M. J.; Heyd, J.; Brothers, E. N.; Kudin, K. N.; Staroverov, V. N.; Kobayashi, R.; Normand, S. S.; Raghavachari, K.; Rendell, A. P.; Burant, J. C.; Iyengar, S. S.; Tomasi, J.; Cossi, M.; Rega, N.; Millam, N. J.; Klene, M.; Knox, J. E.; Cross, J. B.; Bakken, V.; Adamo, C.; Jaramillo, J.; Gomperts, R.; Stratmann, R. E.; Yazyev, O.; Austin, A. J.; Cammi, R.; Pomelli, C.; Ochterski, J. W.; Martin, R. L.; Morokuma, K.; Zakrzewski, V. G.; Voth, G. A.; Salvador, P.; Dannenberg, J. J.; Dapprich, S.; Daniels, A. D.; Farkas, Ö.; Foresman, J. B.; Ortiz, J. V.; Cioslowski, J.; Fox, D. J. *Gaussian 09*; Gaussian, Inc.: Wallingford, CT, USA, 2009.
- (50) Dunning, T. H.; Hay, P. J. *Methods of Electronic Structure Theory*; Plenum Press, 1977; Vol. 2.
- (51) Hariharan, P. C.; Pople, J. A. The influence of polarization functions on molecular orbital hydrogenation energies. *Theor. Chim. Acta* **1973**, *28*, 213–222.
- (52) Francl, M. M.; Pietro, W. J.; Hehre, W. J.; Binkley, J. S.; Gordon, M. S.; DeFrees, D. J.; Pople, J. A. Self-consistent molecular orbital methods. XXIII. A polarization-type basis set for second-row elements. *J. Chem. Phys.* **1982**, *77*, 3654–3665.
- (53) Hay, P. J.; Wadt, W. R. Ab initio effective core potentials for molecular calculations. Potentials for the transition metal atoms Sc to Hg. *J. Chem. Phys.* **1985**, *82*, 270–283.
- (54) Wadt, W. R.; Hay, P. J. Ab initio effective core potentials for molecular calculations. Potentials for main group elements Na to Bi. *J. Chem. Phys.* **1985**, *82*, 284–298.
- (55) Hay, P. J.; Wadt, W. R. Ab initio effective core potentials for molecular calculations. Potentials for K to Au including the outermost core orbitals. *J. Chem. Phys.* **1985**, *82*, 299–310.
- (56) Rassolov, V. A.; Pople, J. A.; Ratner, M. A.; Windus, T. L. 6-31G* basis set for atoms K through Zn. *J. Chem. Phys.* **1998**, *109*, 1223–1229.
- (57) Grimme, S.; Antony, J.; Ehrlich, S.; Krieg, H. A consistent and accurate ab initio parametrization of density functional dispersion correction (DFT-D) for the 94 elements H-Pu. *J. Chem. Phys.* **2010**, *132*, 154104.
- (58) Grimme, S.; Ehrlich, S.; Goerigk, L. Effect of the damping function in dispersion corrected density functional theory. *J. Comput. Chem.* **2011**, *32*, 1456–1465.
- (59) Bordwell, F. G.; Fried, H. E. Heterocyclic aromatic anions with 4n + 2 π-electrons. *J. Org. Chem.* **1991**, *56*, 4218–4223.
- (60) Bordwell, F. G.; Ji, G. Z. Effects of structural changes on acidities and homolytic bond dissociation energies of the hydrogen-nitrogen bonds in amidines, carboxamides, and thiocarboxamides. *J. Am. Chem. Soc.* **1991**, *113*, 8398–8401.
- (61) Webster, R. L.; Noroozi, N.; Hatzikiriakos, S. G.; Thomson, J. A.; Schafer, L. L. Titanium pyridonates and amidates: novel catalysts for the synthesis of random copolymers. *Chem. Commun. (Cambridge, U. K.)* **2013**, *49*, 57–59.
- (62) Choujaa, H.; Cosham, S. D.; Johnson, A. L.; Kafka, G. R.; Mahon, M. F.; Masters, S. L.; Molloy, K. C.; Rankin, D. W. H.; Robertson, H. E.; Wann, D. A. Structural Tungsten-Imido Chemistry: The Gas-Phase Structure of W(NBu^t)₂(NHBu^t)₂ and the Solid-State Structures of Novel Heterobimetallic W/N/M (M = Rh, Pd, Zn) Species. *Inorg. Chem.* **2009**, *48*, 2289–2299.
- (63) Edwards, A.; Hogarth, G.; Hollingsworth, N.; Oller, J. J. Illusive tungsten-imido-dithiocarbamate complexes: Facile carbon–nitrogen bond formation. *Inorg. Chem. Commun.* **2011**, *14*, 1932–1936.
- (64) El-Kadri, O. M.; Heeg, M. J.; Winter, C. H. Film growth precursor development for metal nitrides. Synthesis, structure, and volatility of molybdenum(vi) and tungsten(vi) complexes containing bis(imido)metal fragments and various nitrogen donor ligands. *Dalton Trans.* **2006**, 1943–1953.
- (65) Rische, D.; Baunemann, A.; Winter, M.; Fischer, R. A. Mixed Guanidinato/Alkylimido/Azido Tungsten(VI) Complexes: Synthesis and Structural Characterization. *Inorg. Chem.* **2006**, *45*, 269–277.
- (66) Hsiao, C.-S.; Chen, H.-S.; Hsu, S.-Y.; Wang, T.-Y.; Datta, A.; Lin, C.-H.; Huang, J.-H. Synthesis and characterization of tungsten bis-imido complexes containing bi-dentate pyrrole-amine, pyrrole-imine or ketiminate ligands. *Inorg. Chim. Acta* **2014**, *413*, 1–5.
- (67) Hankin, D. M.; Danopoulos, A. A.; Wilkinson, G.; Sweet, T. K. N.; Hursthouse, M. B. Dalton communications. A new type of sulfenamido ligand. Crystal structure of W(NBu^t)₂(η²-PhSNBu^t)₂. *J. Chem. Soc., Dalton Trans.* **1995**, 1059–1060.
- (68) Motevalli, M.; Parkin, B. C.; Ramnauth, R.; Sullivan, A. C. The first bis(imido) transition metal Schiff-base complexes. *J. Chem. Soc., Dalton Trans.* **2000**, 2661–2662.
- (69) Jeong, H.; Axtell, J. C.; Török, B.; Schrock, R. R.; Müller, P. Syntheses of Tungstentert-Butylimido and Adamantylimido Alkylidene Complexes Employing Pyridinium Chloride As the Acid. *Organometallics* **2012**, *31*, 6522–6525.
- (70) Chidou, V.; Gouzerh, P.; Jeannin, Y.; Olivares, G.; Robert, F.; Hsieh, T. C.; Zubietta, J. Synthesis and x-ray crystallographic characterization of new dinuclear bis(phenyldiazenido)molybdenum complexes [{Mo(C₆H₅N₂)₂X(μ-OR)(C₆H₅NHNH₂)₂}] (X = Cl, OR), [{Mo(C₆H₅N₂)₂(μ-OR)(C₆H₅CONHO)₂}] and [{Mo(C₆H₅N₂)₂Cl(μ-OEt)(EtOH)₂}]. *Polyhedron* **1989**, *8*, 29–38.
- (71) Dreisch, K.; Andersson, C.; Stålhandske, C. Reactions of [WO₂Cl₂(dme)] with tert-butyltrimethylsilylamine—x-ray structure of [W(NBu^t)₂Cl₂(Bu^t-dab)] (Bu^t-dab = N,N'-dit-*t*-butyl-1,4-diaza-1,3-butadiene). *Polyhedron* **1993**, *12*, 1335–1343.
- (72) Clegg, W.; Errington, R. J.; Hockless, D. C. R.; Redshaw, C. A new tetratungstate, [W₄O₄Cl₁₀(NBu^t)₄]₂, and its degradation to the mononuclear complex [WOC₂(NBu^t)-(bipy)] or [WCl₂(NBu^t)₂(bipy)] (bipy = 2,2[prime or minute]-bipyridine). *J. Chem. Soc., Dalton Trans.* **1993**, 1965–1971.
- (73) Allen, F. H.; Kennard, O.; Watson, D. G.; Brammer, L.; Orpen, A. G.; Taylor, R. Tables of bond lengths determined by X-ray and neutron diffraction. Part 1. Bond lengths in organic compounds. *J. Chem. Soc., Perkin Trans. 2 (1972-1999)* **1987**, S1–S19.
- (74) Ciszewski, J. T.; Harrison, J. F.; Odom, A. L. Investigation of Transition Metal–Imido Bonding in M(NBu^t)₂(dpma). *Inorg. Chem.* **2004**, *43*, 3605–3617.
- (75) Odom et al. computationally investigated the energy associated with the bending of imido ligands in related complexes and found that there is a small (2.04 kcal/mol) energy difference between bending angles of 145° and 175°.
- (76) Nugent, W. A.; Mayer, J. M. *Metal-ligand multiple bonds: the chemistry of transition metal complexes containing oxo, nitrido, imido, alkylidene, or alkylidyne ligands*; Wiley, 1988.
- (77) See SI for discussion.
- (78) Nugent, W. A.; Haymore, B. L. Transition metal complexes containing organoimido (nr) and related ligands. *Coord. Chem. Rev.* **1980**, *31*, 123–175.
- (79) Dispersion correction was completed for all isomers of complexes 3 and 6. While quantitative values do change with the inclusion of dispersion (Table S2), the energetic ordering of the isomers agreed with the calculations that did not use dispersion corrections.
- (80) Nugent, W. A. Synthesis of some d0 organoimido complexes of the early transition metals. *Inorg. Chem.* **1983**, *22*, 965–969.

(81) Chan, D. M. T.; Fultz, W. C.; Nugent, W. A.; Roe, D. C.; Tulip, T. H. Homogeneous models for propylene ammoxidation. 1. Tungsten(VI) imido complexes as models for the active sites. *J. Am. Chem. Soc.* **1985**, *107*, 251–253.

(82) Schoettel, G.; Kress, J.; Osborn, J. A. A simple route to molybdenum-carbene catalysts for alkene metathesis. *J. Chem. Soc., Chem. Commun.* **1989**, 1062–1063.

(83) Lentz, M. R.; Fanwick, P. E.; Rothwell, I. P. Formation of novel diaza-metallacycles by insertion of tungsten(ii) aryloxides into aromatic diazine rings. *Chem. Commun. (Cambridge, U. K.)* **2002**, 2482–2483.

(84) Payne, P. R.; Thomson, R. K.; Medeiros, D. M.; Wan, G.; Schafer, L. L. Synthesis, structure, and reactivity of tris(amidate) mono(amido) and tetrakis(amidate) complexes of group 4 transition metals. *Dalton Trans.* **2013**, *42*, 15670–15677.

(85) Danopoulos, A. A.; Wilkinson, G.; Hussain-Bates, B.; Hursthouse, M. B. Dilithium tetra(*t*-butylimido)-molybdate(VI) and -tungstate(VI) and some reactions thereof. X-Ray crystal structures of $W[(\mu\text{-NBu}^t)_2\text{AlX}_2]_2$ ($X = \text{Cl}$ or Me), $[W(\text{NBu}^t)_2(\text{NH}_2\text{Bu}^t)\text{Cl}(\mu\text{-Cl})]_2$, and $[W_2\text{Cu}_5(\text{NBu}^t)_2(\mu\text{-NBu}^t)_6(\text{NHBu}^t)_2]\text{BF}_4$. *J. Chem. Soc., Dalton Trans.* **1990**, 2753–2761.

(86) Bradley, D. C.; Howes, A. J.; Hursthouse, M. B.; Runnacles, J. D. The preparation and properties of some tertbutylimidotungsten(VI) complexes. The X-ray crystal structure of $[W(\text{NBut})(\text{OBut})_3\text{Cl}(\text{NH}_2\text{But})]$. *Polyhedron* **1991**, *10*, 477–482.

(87) Rische, D.; Baunemann, A.; Winter, M.; Fischer, R. A. Mixed Guanidinato/Alkylimido/Azido Tungsten(VI) Complexes: Synthesis and Structural Characterization. *Inorg. Chem.* **2006**, *45*, 269–277.

(88) An overlay of the metal center and coordinated atoms illustrates how similar the amidate and pyridonate structures are in complexes **9** and **12** and is shown in the [Supporting Information](#).

(89) Addison, A. W.; Rao, T. N.; Reedijk, J.; van Rijn, J.; Verschoor, G. C. Synthesis, structure, and spectroscopic properties of copper(II) compounds containing nitrogen-sulphur donor ligands; the crystal and molecular structure of aqua[1,7-bis(N-methylbenzimidazol-2[prime or minute]-yl)-2,6-dithiaheptane]copper(II) perchlorate. *J. Chem. Soc., Dalton Trans.* **1984**, 1349–1356.

(90) Leitch, D. C.; Platel, R. H.; Schafer, L. L. Mechanistic Elucidation of Intramolecular Aminoalkene Hydroamination Catalyzed by a Tethered Bis(ureate) Complex: Evidence for Proton-Assisted C–N Bond Formation at Zirconium. *J. Am. Chem. Soc.* **2011**, *133*, 15453–15463.